




Jurassic to early Cretaceous geodynamic evolution of the eastern Hellenides

Evripidis Mposkos¹ · Alexander Krohe² · Craig Walton^{3,4} · Ioannis Baziotis⁵ 

Received: 9 November 2022 / Accepted: 4 November 2023 / Published online: 2 December 2023
© The Author(s) 2023

Abstract

Remarkably well-preserved crustal sections from the Eastern Hellenides offer the chance to evaluate the regional geodynamic evolution of continental crust. Here, we identify and geodynamically interpret eclogite facies metamorphism in the Triassic–Jurassic volcano-sedimentary series of the West Circum Rhodope zone in the eastern Hellenides. Equilibrium phase diagrams and measured mineral compositions were used to inform reconstructions of geodynamic evolution during the early Alpine period. We newly define the existence of the Eohellenic HP belt, consisting of pre-Alpine basement, continental volcano-sedimentary formations, and a Jurassic magmatic arc. We suggest that the Eohellenic HP-Belt was subducted in the late Jurassic to early Cretaceous beneath the European plate margin. Detailed geodynamic reconstructions such as ours provide a robust anchor for future computational models of long-term crustal evolution in the Eastern Hellenides.

Keywords Rhodope · Eclogites · Thermobarometry · Pseudosections · Hellenides · High-pressure · Metamorphism

Introduction

Petrology, structures and microfabrics of high pressure (HP) metamorphic rocks exposed at Earth's surface provide direct information on the kinematics of earlier material movements in the subsurface. By interpreting these features, we can trace the passage of preserved rocks along subduction and collision zones, from upper crustal to mantle depths, revealing the physical conditions under which those movements take place. Such data are key for reconstructing paleo-plate configurations and hence paleogeography. However, fossilized subduction interfaces that are contiguously exposed

over large areas are rare. This is largely because corresponding HP mineral phases and microfabrics have been overprinted by later tectono-metamorphic processes.

The North-Eastern Hellenides represent a part of the Alpine-Himalayan collision zone encompassing a series of Triassic to early Cretaceous tectonic events:

(i) rifting and ocean formation between the northern margin of Gondwana and the southern margin of paleo-Europe (Vardar/Axios Ocean; e.g. Bortolotti et al. 2012 and references therein, Brown and Robertson 2003; Bonev et al. 2019a and references therein; Mposkos et al. 2021); (ii) northward intra-oceanic subduction within the Vardar/Axios Ocean and sequential fore arc and arc magmatic activity (Paikon–Chortiatis magmatic arc (PCMA) at the front of a continental fragment rifted off the European margin (Vertiskos-Ograzden complex-VOC), Mercier 1968; Brown and Robertson 2003; Bortolotti et al. 2012; Bonev et al. 2015b), and ensialic back-arc extension at the southern margin of paleo-Europe (E-Vardar/Axios Ocean, Bébien et al. 1986; Gallhofer et al. 2017; Boev et al. 2018; Mposkos et al. 2021); (iii) obduction of ophiolites of the W-Vardar/Axios Ocean over the Adriatic continental margin (Pelagonia zone), and, finally; (iv) subduction/collision of the Pelagonia zone and rifted European continental blocks with paleo-Europe creating the HP metamorphic belt(s) depicting the early Cretaceous suture (e.g. Kiliass et al. 2010; Krenn et al.

✉ Ioannis Baziotis
ibaziotis@aua.gr

¹ School of Mining and Metallurgical Engineering, National Technical University of Athens, Athens, Greece

² Institute for Mineralogy, University of Münster, Corrensstrasse 24, 48149 Münster, Germany

³ Department of Earth Sciences, Institute für Geochemie und Petrologie, ETH Zurich, NW D 81.2, Clausiusstrasse 25, 8092 Zurich, Switzerland

⁴ Trinity College, University of Cambridge, Cambridge CB21TQ, UK

⁵ Laboratory of Mineralogy and Geology, Agricultural University of Athens, Iera Odos 75, 11855 Athens, Greece

2010; Burg 2012; Schenker 2013; Nitra et al. 2018 and references therein).

The suture is overprinted by:

(i) Middle-late Cretaceous extension, as indicated by the middle Cretaceous transgression and late Cretaceous neritic to pelagic carbonate sedimentation in the Pelagonia, Almopias and Paikon zones (Mercier 1968; Brown and Robertson 2003; Sharp and Robertson 2006; Kiliyas et al. 2010); (ii) late Cretaceous–early Tertiary subduction/collision and emplacement of the Gondwana-derived Adriatic plate underneath the European continental margin (that then consisted of paleo-Europe and material already accreted in the late Jurassic–early Cretaceous) as well as (iii) post-collisional back-arc extension creating the Aegean Sea (e.g. Dinter 1998; Froitzheim et al. 2014; Brun and Sokoutis 2018 and references therein).

As a result of back-arc extension, the thickened crustal bulge of the Rhodope metamorphic domain (RMD) has been exposed, revealing the deep interior of the collisional belt. Thus, the record of late Jurassic–early Cretaceous (early Alpine) deep-seated tectonic processes is well-preserved and unambiguously discernible through shallow and deep structural levels of the orogenic edifice.

In this study we focus only on the Mesozoic events recorded in the intercalations of the West Circum Rhodope zone (W-CRZ) within the Vertiskos-Ograzden complex (VOC). Mposkos et al. (2021) have discussed the metamorphic and microfabric record of the VOC part in Greece. We used optical microscopy and electron probe microanalysis, to characterise the petrographic relations and to obtain mineral chemistry data from the minerals occurring within eclogite and metapelite samples from the studied area.

We coupled our data with equilibrium phase diagrams (pseudosections) to constrain the peak pressures and temperatures conditions and to define a tentative decompression path. Based on our data along with critical review of the existing literature, we argue for the presence of an oceanic branch of the Neotethys Ocean between the VOC and the south European margin, which closed in late Jurassic simultaneously with the northeast subduction of the W-Vardar Ocean. We discuss a scenario concerning the location of the oceanic basin from which the E-Vardar ophiolites derive. Subsequently, we present a geodynamic reconstruction that links the W-CRZ and the middle-late Jurassic Paikon–Chortiatis magmatic arc with the structurally higher tectono-metamorphic complexes (Segments I and II) of the central and eastern Rhodope Metamorphic Domain (RMD) (see discussion).

Present-day structural relationships

The term RMD comprises high- and medium-grade HP-metamorphic rocks in the central and eastern sections of the study area (Fig. 1). The southwestern part of the RMD

consists of the VOC. It extends from eastern Central Macedonia of northern Greece, into eastern North Macedonia and SW Bulgaria (Fig. 1a) and represents the uppermost tectonic unit of the RMD (Kockel and Mollat 1977; Ricou et al. 1998; Burg 2012; Kydonakis et al. 2014; Fig. 1b,c). The VOC predominantly consists of a pre-Alpine (Proterozoic–Paleozoic) continental crust affected by Variscan HP/UHP-metamorphism (~334 Ma), followed by partial melting and migmatite formation during decompression (~321 Ma) (Himmerkus et al. 2009a; Peytcheva et al. 2015; Trapp et al. 2020 and references therein), rift related Triassic low pressure-high temperature (LP-HT) metamorphism associated with bimodal plutonic and volcanic magmatism (240–222 Ma) (Mposkos et al. 2021; Himmerkus et al. 2009b; Bonev et al. 2019a and references therein), and late Jurassic–early Cretaceous moderate high pressure (MHP) metamorphism (Kydonakis et al. 2016; Mposkos et al. 2021). A fourth, LP-amphibolite facies overprinting metamorphic event is recorded only in the easternmost VOC (Dixon and Dimitriadis 1987; Mposkos et al. 2021). These metamorphic events reflect Variscan terrane amalgamation, Triassic rifting and early alpine collision respectively. In the late Cretaceous, the VOC was emplaced in the upper crust (Wuthrich 2009; Kydonakis et al. 2014).

To the east, in the central and eastern RMD, the VOC is underlain by Segment I, Segment II and Segment III (Krohe and Mposkos 2002), that largely correspond to the Upper-, Middle-, and Lower Allochthon, according to Janák et al. (2011). Segment I and II contain pre-Alpine, late Jurassic magmatic arc and mid ocean protoliths (e.g. Bonev et al. 2013, 2015a; Turpaud and Reischman 2010; von Quadt et al. 2009; Froitzheim et al. 2014; Pleuger et al. 2020) and were subjected to late Jurassic–early Cretaceous HP-HT metamorphism, partial melting and migmatization during decompression (~150–117 Ma, Liati et al. 2011 and references therein; Bauer et al. 2007; Georgieva et al. 2010; Bosse et al. 2009; Kirchenbauer et al. 2012; Wawrzenitz et al. 2015; Georgiev et al. 2016). In both segments, pelitic garnet-kyanite gneisses contain diamond inclusions in garnet recording UHP metamorphism (e.g. Petrik et al. 2016 and references therein). Electron microprobe U-Th-Pb monazite dating yielded mean ages of ~200 Ma, which are interpreted as indicative of the timing of the ultra-high pressure (UHP) metamorphic event. This event occurred during the late Triassic to early Jurassic and was associated with the collision and subduction of continental crust subsequent to the closure of the Palaeotethys Ocean (Petrik et al. 2016).

Segment I and Segment II were subjected to overprinting amphibolite facies metamorphism and wet melting in upper Cretaceous (~78–69 Ma) and middle Eocene (~50–55 Ma) respectively (Liati et al. 2011, 2016; Bauer et al. 2007; Wawrzenitz et al. 2015; Gautier et al. 2017 and references therein). Clinzoisite bearing muscovite pegmatites with

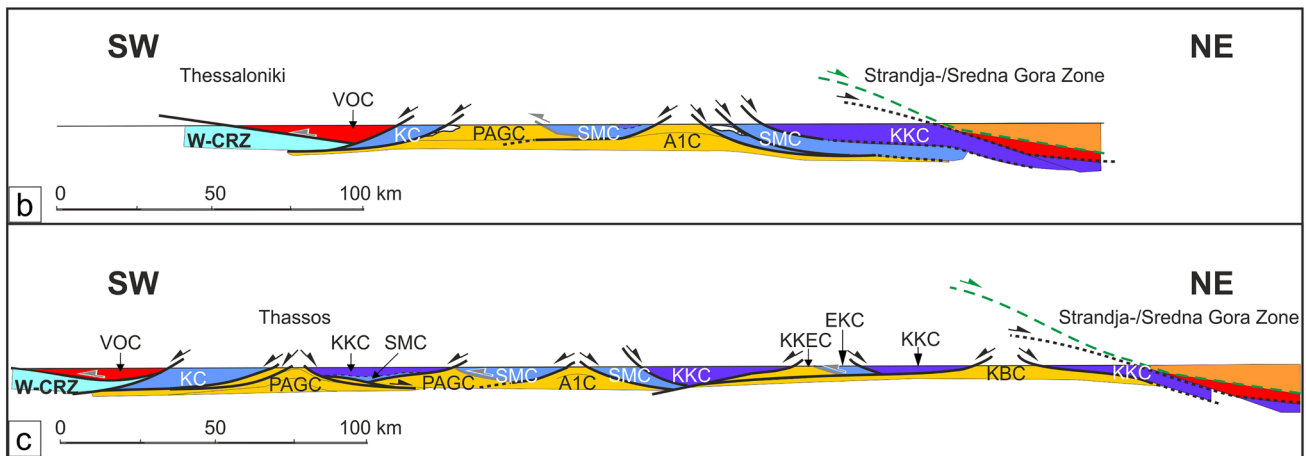
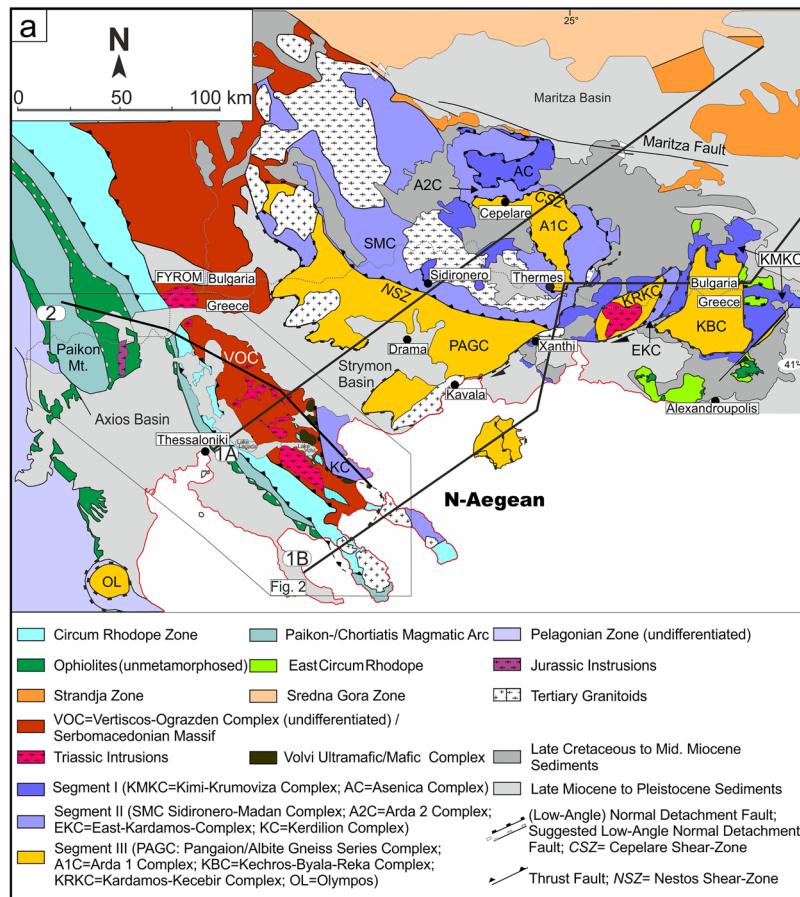


Fig. 1 a Tectonic map of the Rhodope Metamorphic Domain (including the Serbomacedonian Massif) the “Central Macedonian HP Belt” and the E-Vardar/Axios ophiolite zone adapted from Mposkos et al.

(2021)(modified from Jahn-Awe et al. 2010; Kockel and Mollat 1977). b, c Geological sections along the lines shown in 1A and 1B

crystallization ages of 65–62 Ma intruded Segment I (Mposkos and Wawrzenitz 1995; Liati et al. 2002). Between 62 Ma and the middle Eocene Segment I was lifted to the upper crust and juxtaposed against the eastern VOC along an extensional detachment fault (Krohe and Mposkos 2002; Brun and Sokoutis 2007; Fig. 1). The underlying Segment II (Sidironero complex), which stayed in the middle crust at

that time, was exhumed after c. 38 Ma (Bosse et al. 2009; Nagel et al. 2011; Wawrzenitz et al. 2015).

The structurally lowermost levels (Segment III) represent the Apulian plate (Dinter 1998; Mposkos and Krohe 2000; Jahn-Awe et al. 2010; Froitzheim et al. 2014). The metamorphic record of Segment III involves relicts of Variscan events (Mposkos and Wawrzenitz 1995) as well as HP metamorphic

and tectonic events related to late Cretaceous subduction of oceanic crust (Miladinova et al. 2018) and Cenozoic collision of Apulia with the European plate margin (Jahn-Awe et al. 2010; Froitzheim et al. 2014; see also re-interpretation of the Eocene eclogite ages published in Miladinova et al. 2018). Segment III correlates with the HP metamorphic units of the Cycladic belt (Mposkos et al. 2012; Froitzheim et al. 2014).

The late Jurassic–early Cretaceous eclogite and HP-granulite facies metamorphisms (149–119 Ma) in Segments I and II overlap with the early Cretaceous (132 Ma) low amphibolite facies overprint of the MHP metamorphism in VOC and the greenschist facies overprint (124–126 Ma) of the HP/LT metamorphism in the W-CRZ (Kydonakis et al. 2015, 2016; Mposkos et al. 2021; Figs. 1, 2b).

To the west, in the western RMD, the structural relationships between the VOC and adjoining tectonic units are less clear (Fig. 1). In Central Macedonia of northern Greece (Fig. 2), the W-CRZ and the Chortiatis magmatic suite bound the VOC to the west (Kockel and Mollat 1977; Kockel et al. 1977; Asvesta and Dimitriadis 2010; Kydonakis et al. 2015). Kockel et al. (1977) and Kydonakis et al. (2015) interpret the two mica-gneisses and schists lying between W-CRZ and Chortiatis magmatic suite as tectonic slivers of the VOC. They consider the W-CRZ as the Mesozoic cover of the VOC. The Paikon magmatic suite to the west of the Axios Neogene basin (Fig. 1) is interpreted as a continuation of the Chortiatis magmatic suite (Anders et al. 2005; Zachariadis 2007).

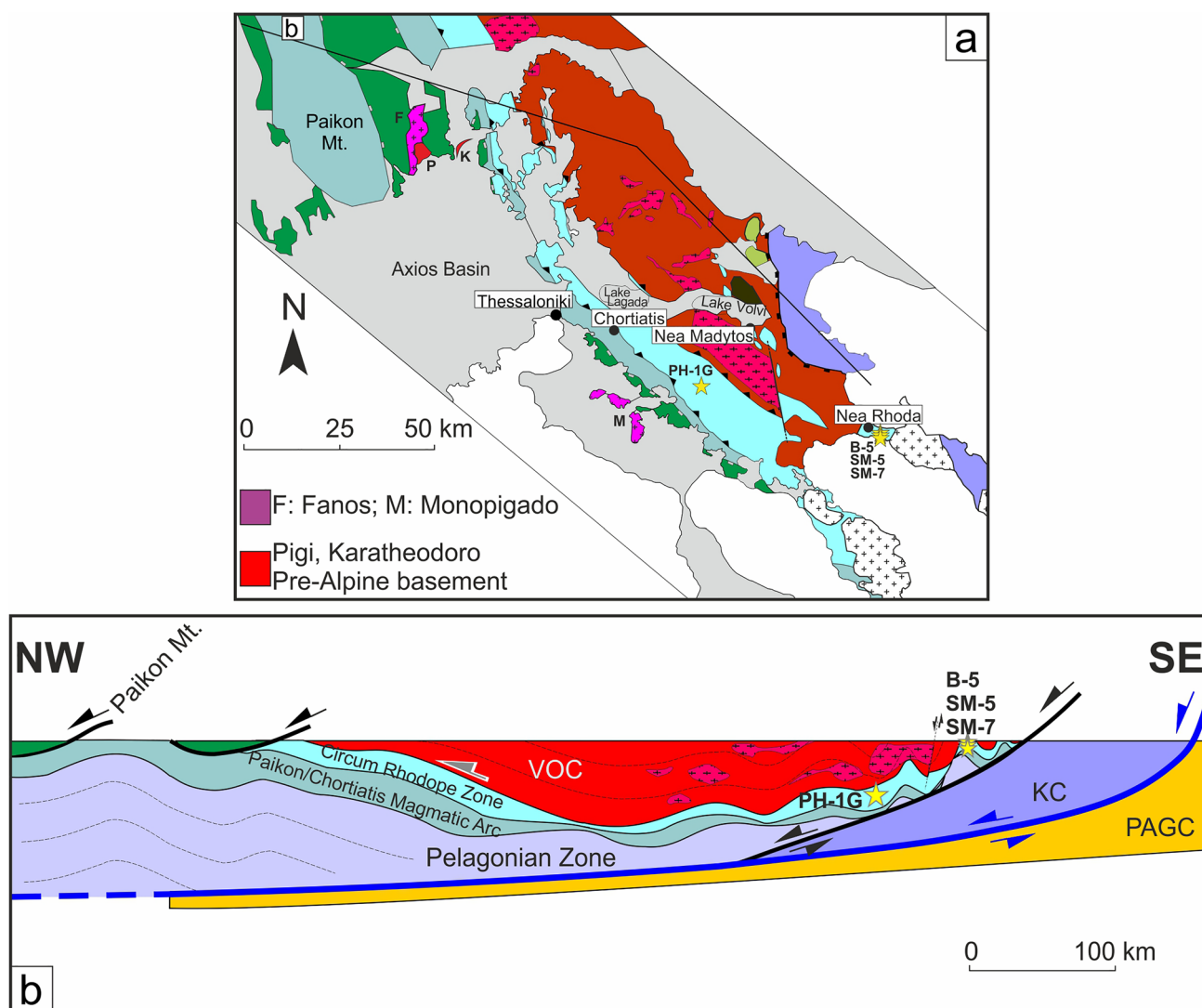


Fig. 2 **a** Simplified geological map of the “Central Macedonian HP Belt”, the E-Vardar/Axios ophiolite zone, the Vertiskos complex and the surroundings, after Kockel and Mollat (1977)(with additions

and modifications). Stars are localities of the samples studied in this work. P: Pigi, K: Karathodoro continental slivers; F:Fanos; M: Monopigado. **b** Geological section along the line B shown in A

Following this interpretation, we refer to both magmatic suites as Paikon–Chortiatiss magmatic arc (PCMA) in this work. W-CRZ and PCMA consist of Triassic–Jurassic turbiditic and meta-volcano-sedimentary sequences, respectively (Mercier 1968; Kockel et al. 1977; Meinhold et al. 2009; Brown and Robertson 2003). In the late Jurassic–early Cretaceous, concurrently with the VOC they were subjected to HP/LT metamorphism (Michard et al. 1994; Baroz et al. 1987; Kydonakis et al. 2015). In the eastern VOC meta-volcanic and -sedimentary sequences are intercalated (Fig. 2). These rocks record eclogite facies metamorphism and lower amphibolite facies overprinting during decompression (Kydonakis et al. 2015). Unlike to VOC, they show only one tectono-metamorphic event, hence lacking the Variscan and Triassic metamorphic history of the VOC. They are interpreted as tectonic intercalations W-CRZ in the pre-Alpine basement of the VOC (Kockel et al. 1977; Dixon and Dimitriadis 1984; Kydonakis et al. 2015).

Farther to the west, the E-Vardar/Axios ophiolite zone (Peonias subzone according to Mercier 1968; Fig. 2), overlies the W-CRZ and PCMA (Mercier 1968; Mercier and Vergely 1994; Figs. 1, 2). The ophiolites (including the Pigi and Karathodoro tectonic slivers, see discussion), occupy the structurally uppermost position in the study area. They are relicts of the E-Vardar/Axios ocean that has formed in middle-late Jurassic (~169–149 Ma) in a back-arc and arc setting (Bébien et al. 1987; Zachariadis 2007; Božović et al. 2013; Bonev et al. 2015b). Dextral strike-slip tectonics characterizes the tectonic contact of the ophiolites to the Chortiatiss magmatic arc and W-CRZ (Ricou et al. 1998; Tranos et al. 1999). The dearth of any sign of post-magmatic (pressure accentuated) metamorphism in E-Vardar/Axios ophiolites (other than hydrothermal alteration), indicates that this ophiolite complex stayed near the surface since its formation in the late Jurassic (Mercier 1968; Kockel et al. 1977; Bonev et al. 2015b). More details for the W-CRZ and the PCMA are discussed in a separate section supplementary text.

Results

Field relations

In the area southeast of Nea Roda village and below the Neogene deposits occur anatectic two mica gneisses, serpentinites, amphibolites and garnet mica schists (Kockel et al. 1978a, b, c; Bonev et al. 2019a; and our field observations). Himmerkus et al. (2012) involve these rocks in their “mélange zone”. Foliation planes mainly trend NE–SW dipping to NW. The upper tectono-stratigraphic lithologies are comprised of anatectic gneisses and serpentinite, whereas the lower ones consist of amphibolites and metapelites. At places, the foliation planes are vertical (Kockel et al. 1978a,

b, c and our observations). To the southwest, the garnet mica schists are in contact with the 44 Ma old Ouranoupolis granodiorite (Himmerkus et al. 2012). Garnet mica schists and amphibolites were subjected to lower grade of metamorphism (low amphibolite facies, see below) compared to the overlying anatectic gneisses and similar grade with the metapelites from the areas of Volvi-lake and Nea Madytos (Sakellariou and Dürr 1993; Kydonakis et al. 2015). The garnet mica schists, marbles, quartzites and amphibolites (including the eclogite body studied in this work) of Nea Roda represent the southeastern outcrop of the tectonically intercalated W-CRZ in VOC (Fig. 2).

Petrography and mineral chemistry

Garnet-kyanite-staurolite-mica schists (sample B-5)

The metapelite *sample B-5* shows compositional layering with alternating pelitic and quartzitic (meta-chert) layers in the scale of a few centimeters. Major phases are muscovite, quartz, garnet, kyanite, chlorite and plagioclase. Biotite and staurolite (~1 vol%) are minor phases. Accessory minerals are tourmaline, ilmenite, rutile, apatite, and zircon. The pelitic layers are rich in garnet and kyanite porphyroblasts up to 0.8 and 1.5 cm in size, respectively (Fig. 3a, b). A deformation that overprints the compositional layering created a foliation that extends sub-parallel to the layering. Quartzite layers had a higher viscosity as they show lens shape and pinch and swell structures and tight folds (Fig. 3a-b).

Garnet (~5–8 vol%) appears as euhedral to subhedral porphyroblasts up to 0.8 cm in diameter. Garnet contains inclusions of quartz, clinozoisite, ilmenite, rutile, margarite, tourmaline, and of composite grains consisting of muscovite, biotite and quartz (Fig. 3c-e). Ilmenite and clinozoisite inclusions occur in the core and rutile inclusions in the mantle of the garnet (Fig. 3c). At the rim, garnet is replaced by chlorite, plagioclase and biotite (Fig. 3f). Garnet contains a relict internal foliation defined by trails of quartz, ilmenite and an impressive amount of tourmaline. The internal foliation of the garnet continues into the external foliation defined by basal plane preferred orientation of muscovite and the extension of quartz-rich bands.

Kyanite porphyroblasts (~4–6 vol%) are up to 1.5 cm in length. They contain inclusions of tourmaline, rutile, muscovite and ilmenite (Fig. 4a). Rutile and tourmaline inclusions in kyanite are aligned parallel to each other forming an internal foliation. Rutile inclusions in turn contain inclusions of ilmenite (Ilm-1) (mineral abbreviations after Whitney and Evans 2010). Aggregates of small flakes of muscovite, or muscovite, chlorite and staurolite replaced the kyanite (Fig. 4b, c). Matrix rutile is replaced by ilmenite (Ilm-2). Kyanite shows deformation kinks.

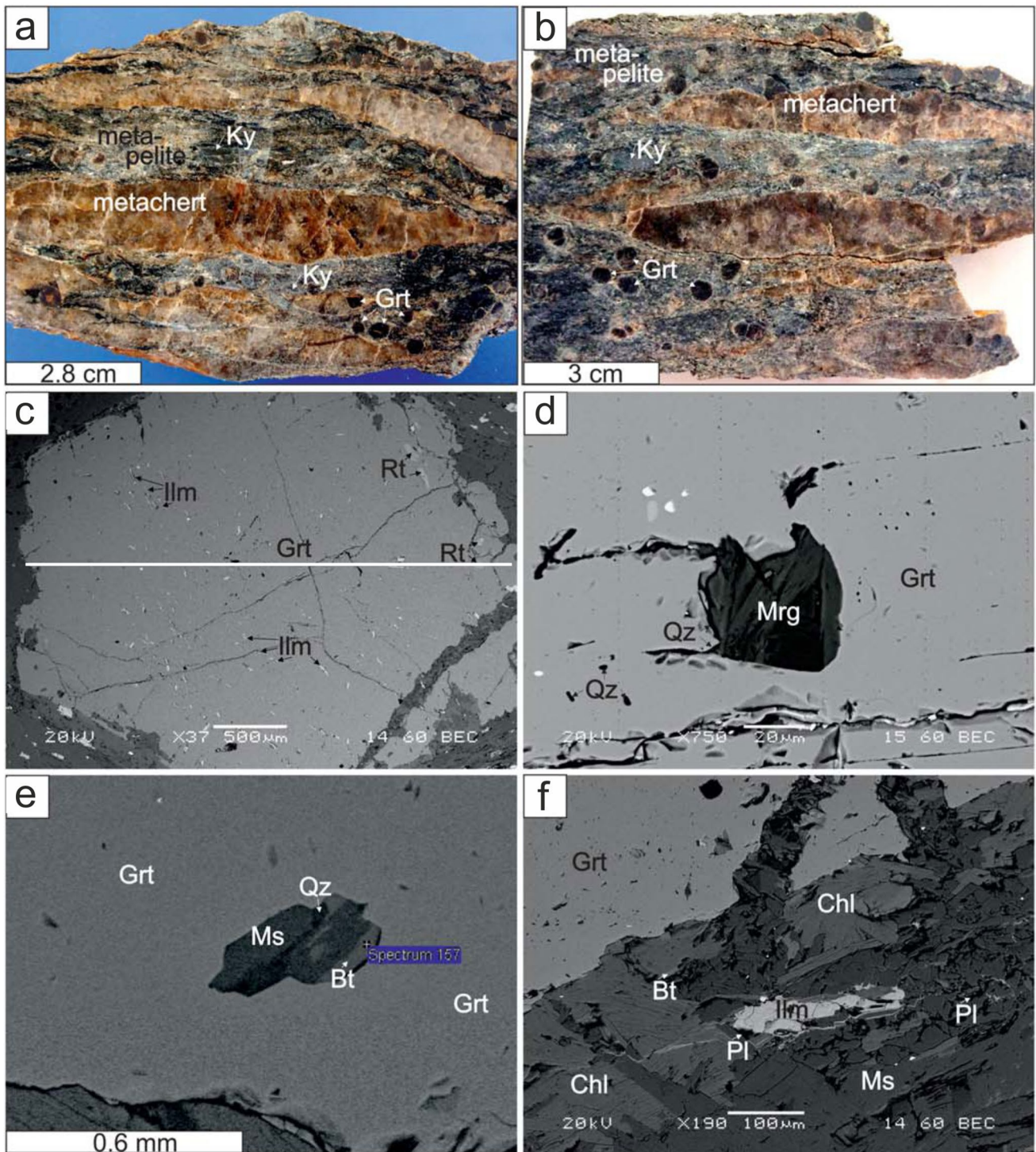


Fig. 3 Garnet-kyanite-metapelite B-5. **a, b** Hand specimen showing intercalations of quartzite (meta-chert) lenses. The pelitic layers contain garnet and kyanite porphyroblasts up to 0.8 and 1.5 cm respectively. **c** Garnet porphyroblast containing inclusions of ilmenite and rutile. The ilmenite inclusions occur in the core and the rutile inclu-

sions in the outer mantle of the garnet. The white line indicates the compositional rim-rim profile given in Fig. 5. **d** Margarite and quartz inclusions in garnet. **e** Composite inclusion in garnet consisting of muscovite, biotite and quartz. **f** Garnet is replaced by chlorite, plagioclase and biotite. **c–f** SEM pictures

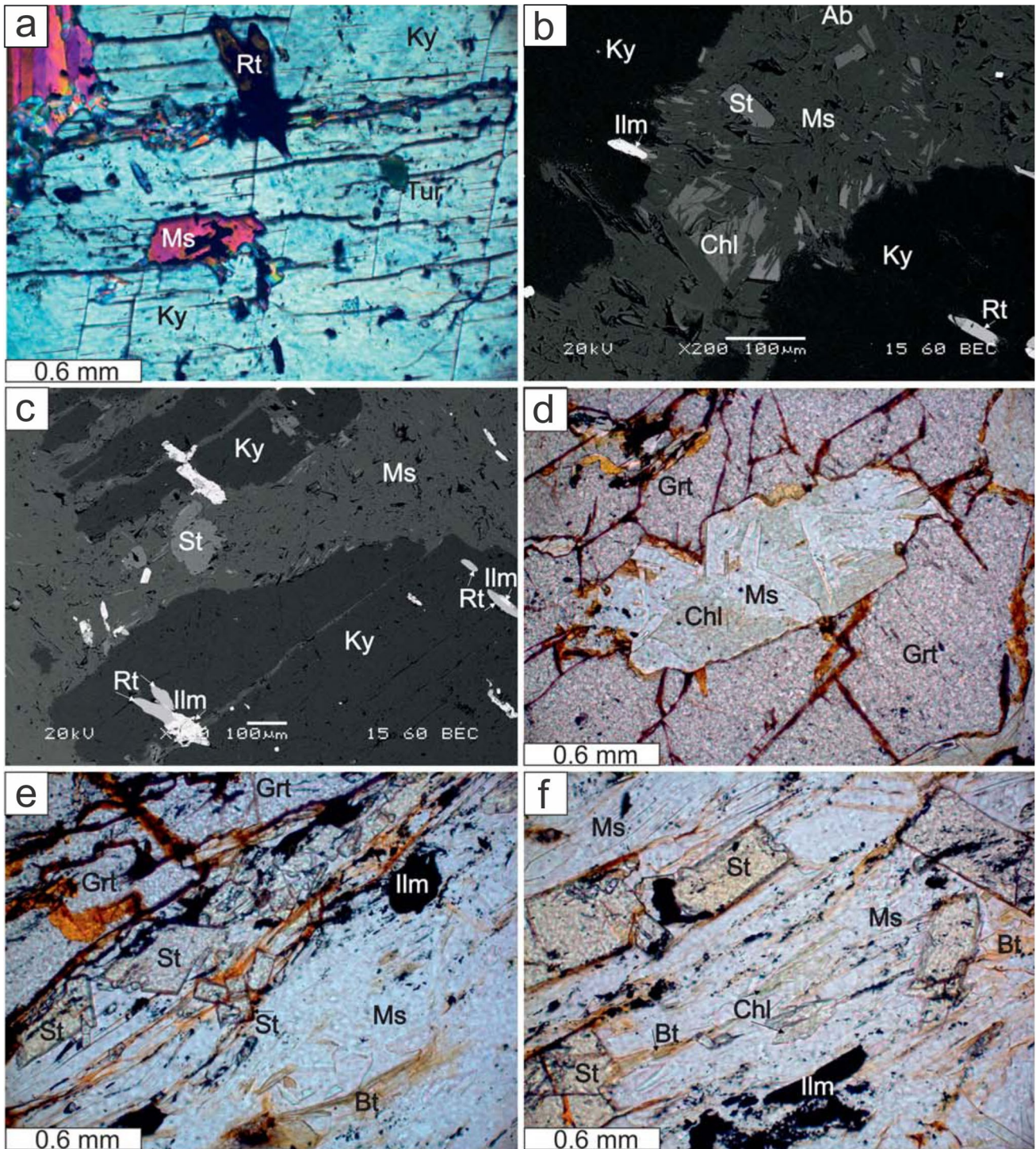


Fig. 4 Garnet-kyanite-metapelite B-5. **a** Kyanite with inclusions of muscovite, rutile and tourmaline. The muscovite inclusion contains inclusions of ilmenite. **b, c** Kyanite porphyroblast replaced from staurolite, muscovite and chlorite. The kyanite contains inclusion of rutile. At the replaced part of the kyanite former rutile inclusion in kyanite is replaced from ilmenite. Along the kyanite cleavage plane

the rutile inclusion is replaced by ilmenite. Garnet staurolite metapelite SM-7. **d** Composite inclusion in garnet consisting of chlorite and muscovite. **e** Staurolite formed along the margins of a garnet porphyroblast. **f** Matrix staurolite associated with muscovite and biotite. **a, d, e, f** microphotographs; **a** crossed polars; **d, e, f** only one polar; **b, c** SEM pictures

The chemical composition of garnet ranges between $\text{Grs}_{9-23}\text{Pyr}_{5-19}\text{Alm}_{67-76}\text{Sps}_{0-5}$. Compositional zoning showing a bell-shaped profile is characteristic for growth zoning (Fig. 5; Table S1). From the core to the rim, grossular and spessartine components decrease and the pyrope component increases. In staurolite, the $\text{Mg}/(\text{Mg} + \text{Fe})$ ratio ($\text{Mg}\#$) is 0.18–0.23, and the ZnO content is 5.78–6.16 wt%. In muscovite inclusions in garnet and kyanite the Si-content ranges from 6.27–6.30 and in matrix muscovite from 6.17 to 6.19 a.p.f.u. (Table S1). The paragonite component in muscovite is 11–16 mol%. Chlorite and biotite show a narrow compositional range. $\text{Mg}\#$ is 0.56 and 0.57; the TiO_2 content in biotite is 1.59–1.64 wt%. Margarite only occurs as inclusion in garnet; the paragonite component is 22–26 mol% (Table S1). Plagioclase (An_{20-26}) associated with chlorite and biotite, replace garnet (Fig. 3f).

Garnet-staurolite-mica schists (SM-7)

Garnet porphyroblasts (up to 6 mm in size) contain inclusions of quartz, muscovite, chlorite, graphite, ilmenite, rutile and composite grains consisting of muscovite and chlorite (Fig. 4d). At the margins garnet porphyroblasts show resorbed edges and are replaced by chlorite and staurolite (Fig. 4e). Staurolite also occurs in domains, where garnet is not present (Fig. 4f). It is associated with chlorite, muscovite and biotite. Two generations of chlorite are present. Chl-1 are inclusions in garnet and occur as major phase in the matrix associated with muscovite. At the margin, this chlorite is replaced by biotite. Chl-2 is retrograde replacing garnet and biotite. The Ti-phase in the matrix is ilmenite. Matrix rutile is completely replaced by ilmenite. Ilmenite also occurs as inclusions in staurolite.

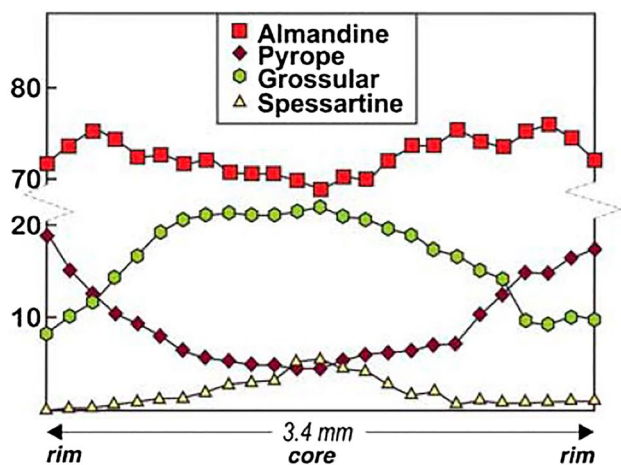


Fig. 5 Compositional profile of garnet porphyroblast from the garnet-kyanite metapelite B-5

Eclogite (SM-5)

The eclogite SM-5 crops out as a narrow (50 × 100 m), isolated hummock beneath the alluvials (Dimitriadis and Godelitsas 1991). Garnet and omphacite constitute more than 90 vol%; barroisite, ferro-pargasite (amphibole nomenclature after Leake 1997) and rutile are ~5–6 vol% and quartz, paragonite, clinozoisite, allanite and apatite occur in minor amounts. Preiswerkite and Ca-rich paragonite only occur as rare inclusions in garnet. Ca-poor paragonite occurs as inclusion in omphacite. Garnet (0.2–1 mm in size) commonly contains inclusions of rutile and quartz, less commonly pargasite, ferro-pargasite, barroisite, and rarely clinozoisite, titanite, preiswerkite, paragonite and biotite (Fig. 6a, b). Omphacite (0.3–6 mm in size) contains inclusions of garnet, Na–Ca-amphibole (barroisite, magnesio-katophorite), rutile, quartz, paragonite, clinozoisite, allanite and apatite. Matrix Na–Ca-amphibole (barroisite, magnesio-katophorite), ~2 vol% occurs in small grains (0.1–0.3 mm in size) interstitially between garnet and omphacite (Fig. 6c). The major Ti-phase is rutile. It occurs as inclusion in garnet, omphacite, barroisite and in the matrix. Rutile contains inclusions of ilmenite (Ilm-1), quartz and barroisite (Fig. 6c, e). Textures are granoblastic. Isometric garnet and omphacite grains are in textural equilibrium as the ~120° triple junctions indicate (Fig. 6f). In some layers prismatic omphacite forms poikiloblasts up to 6 mm in size, which are rich in garnet and rutile inclusions. Prismatic omphacite grains define a weak lineation.

In samples with a low degree of amphibolitization, retrogression is limited to local replacement of garnet and eclogitic omphacite (Omp-1) by omphacite (Omp-2), Na–Ca-amphibole (katophorite, magnesio-katophorite, taramite, magnesio-taramite), Ca-amphibole (ferro-pargasite, ferro-edenite) and albite (An_{3-7}) (Fig. 7a–f). Omphacite and paragonite are replaced by pargasite and oligoclase (An_{15}) (Fig. 7e). Retrogression of eclogite eventually resulted in complete decomposition of omphacite. In strongly amphibolitized samples, two successive stages of retrogression are observed. *Stage 1* forms symplectites (apparent size 20–30 × 80–120 μm consisting of long prismatic Omp-2-albite and of Ca-amphibole (ferro-pargasite, ferro-edenite, edenite)-albite (An_{3-8}) that replace the Omp-1 blasts. Garnet is replaced by kelyphitic tschermakite, ferro-pargasite and albite and rutile by ilmenite (Ilm-2). *Stage 2* replaces omphacitic clinopyroxene by very thin vermicular symplectites consisting of diopsidic clinopyroxene, magnesio-hornblende, actinolite and oligoclase (An_{12-17}) (Fig. 7h–i). Garnet and kelyphitic tschermakite/ferro-pargasite are replaced by magnesio-hornblende and epidote associated with plagioclase (An_{27}) (Fig. 7j–k). This stage replaced rutile and ilmenite by titanite (Fig. 7j, l).

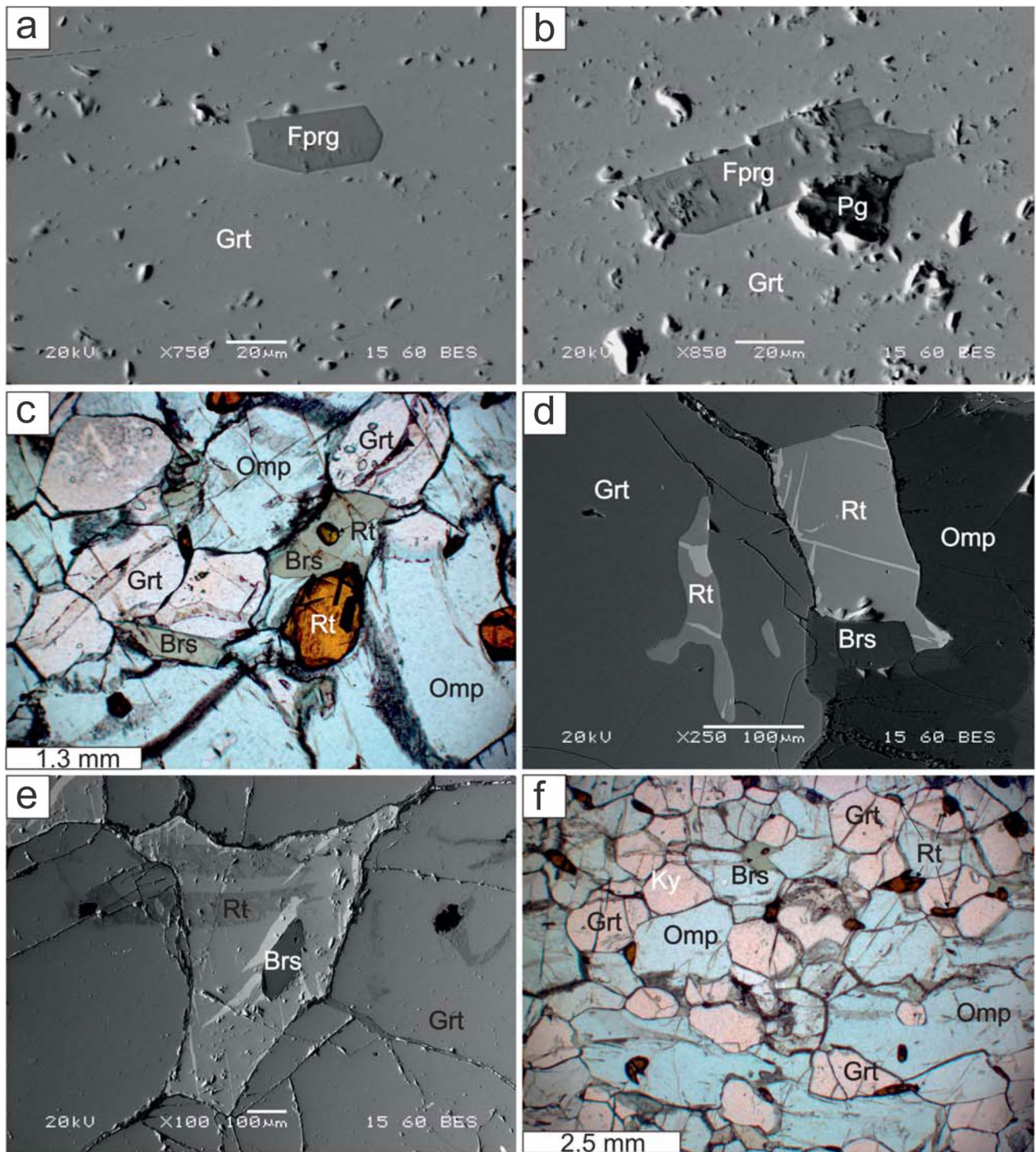


Fig. 6 Eclogite SM-5. **a–b** Inclusions of ferro-pargasite and paragonite in garnet. **c–d** matrix barroisite in textural equilibrium with garnet, omphacite and rutile. **e** barroisite inclusion in rutile. **f** Granoblastic

garnet, omphacite, rutile and barroisite in textural equilibrium. **c, f** microphotograph, only one polar; **a, b, d, e** SEM pictures

Garnet has the composition ($\text{Grs}_{21-25}\text{Pyr}_{18-22}\text{Alm}_{53-56}\text{Sps}_{0.7-1.9}$). Systematic compositional zoning between core and rim in individual grains is not observed (Table S2). The jadeite component of Omp-1 ranges from 43 to 49 mol%.

The jadeite content of Omp-2 that is associated with ferro-pargasite/edenite and albite (An_{3-7}) replacing Omp-1 (Jd_{47} ; Fig. 7a) is 32–33 mol%. The clinopyroxene that is symplectically intergrown with plagioclase (An_{13-17}) is a sodic

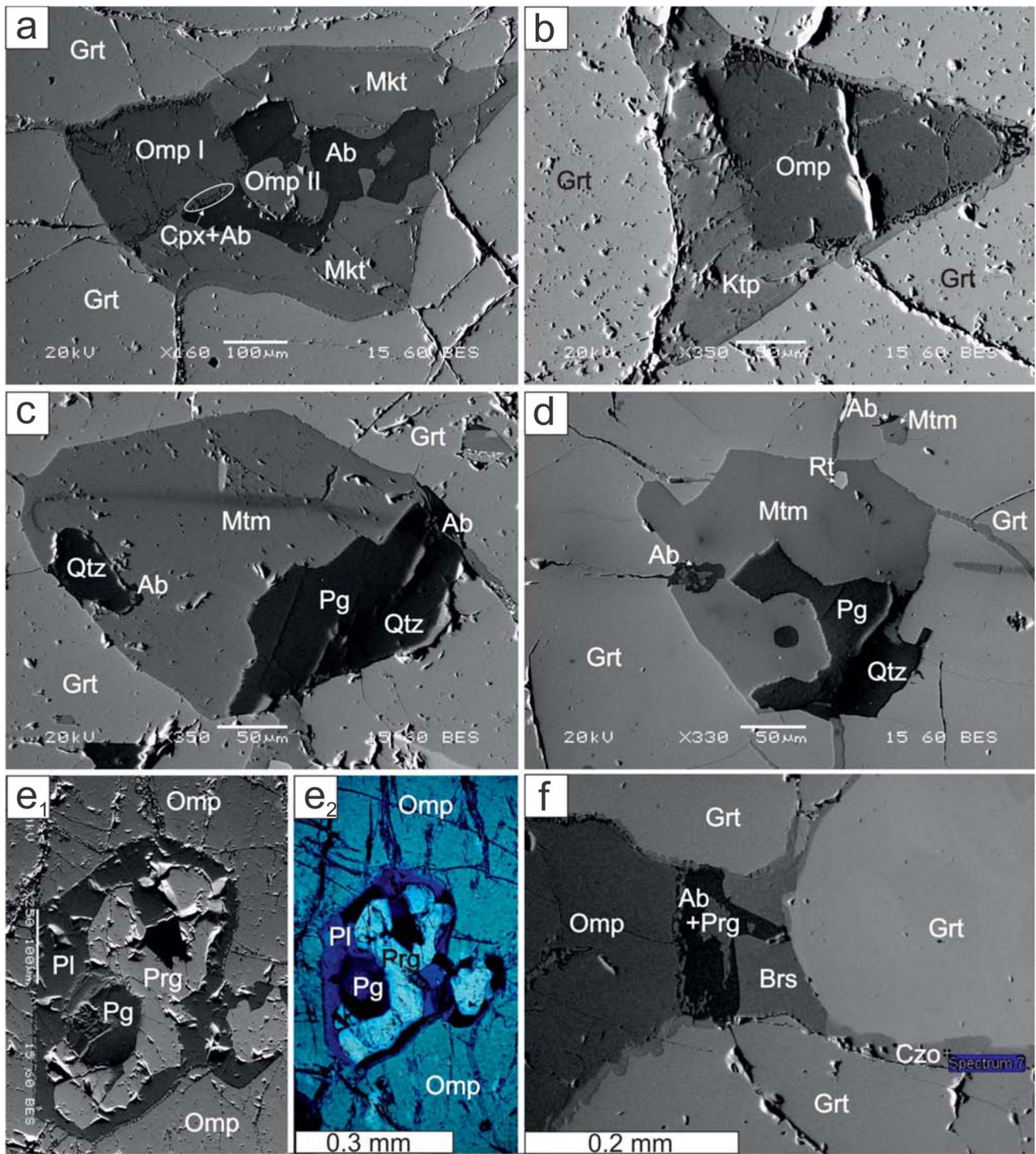


Fig. 7 **a** Omphacite (Omp-1) is decomposed to omphacite with lower jadeite component (Omp-2) and albite. Omphacite and garnet are replaced from magnesio-katophorite. **b** Omphacite and garnet are replaced from katophorite. At the rims, omphacite is replaced by albite-amphibole symplectites. **b1**) Garnet is replaced by kelyphitic katophorite and albite. **c, d** Magnesio-taramite and albite replace garnet, paragonite and former omphacite. **e** Omphacite and paragonite inclusion in omphacite are replaced by pargasite and plagioclase. **f, g** Garnet and omphacite are replaced in two stages: **a**) by kelyphitic bar-

roisite and clinozoisite; **b**) by pargasite and albite symplectites, (Ap: apatite). **h, i** Eclogitic omphacite (Omp-1, Jd_{47}) is decomposed in two stages: **a**) to thick prismatic omphacite (Omp-2, Jd_{33-34})-albite symplectites and ferro-pargasite/ferro-edenite; **b**) Omp-2 to fine grained symplectites consisting of magnesio-hornblende, oligoclase and diopside. **j, k** Garnet is replaced from blue-green Ca-amphibole, epidote and oligoclase. **k, l** Rutile is replaced from ilmenite and ilmenite from titanite coronas. **j, l** Microphotographs, only one polar

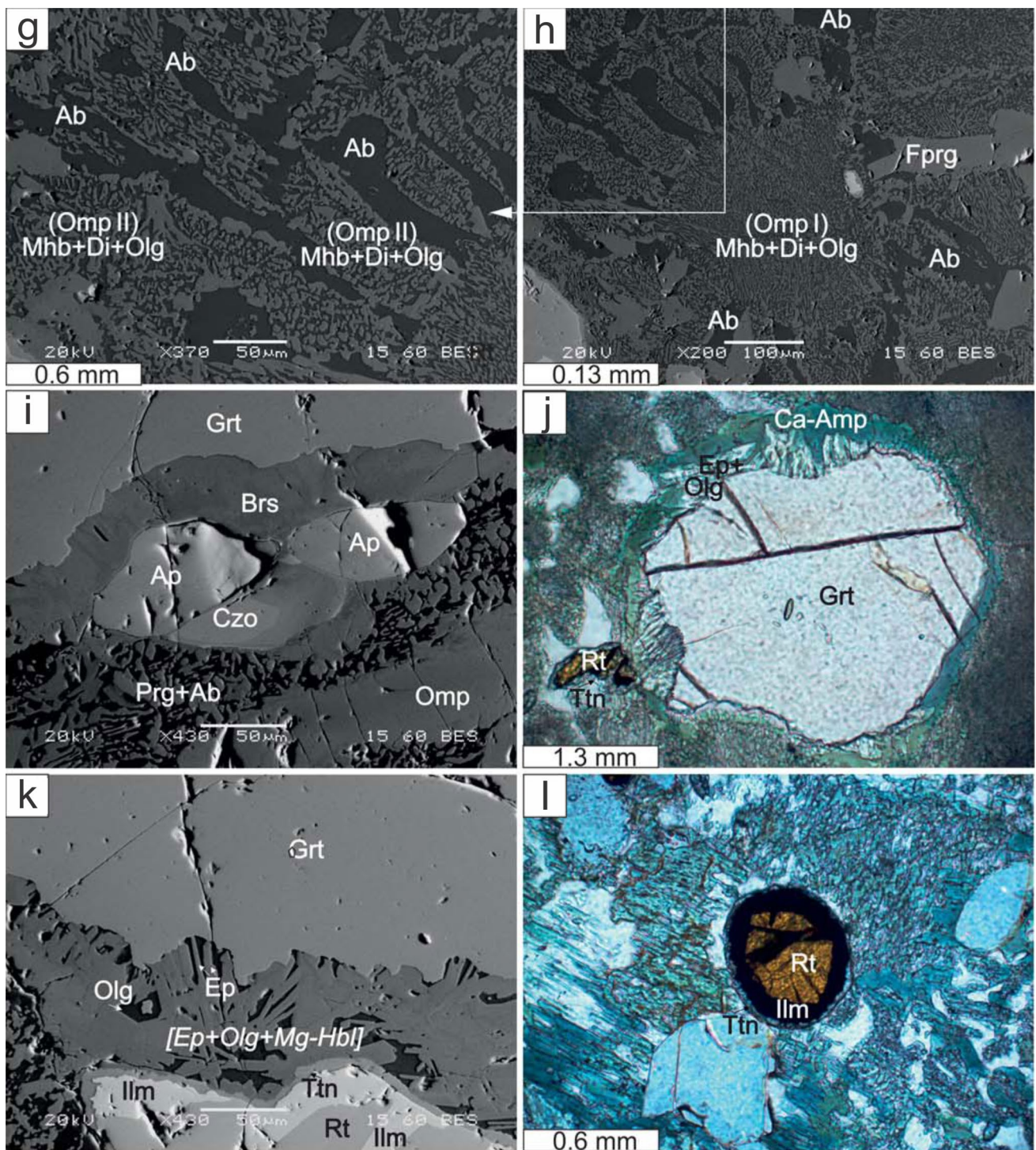
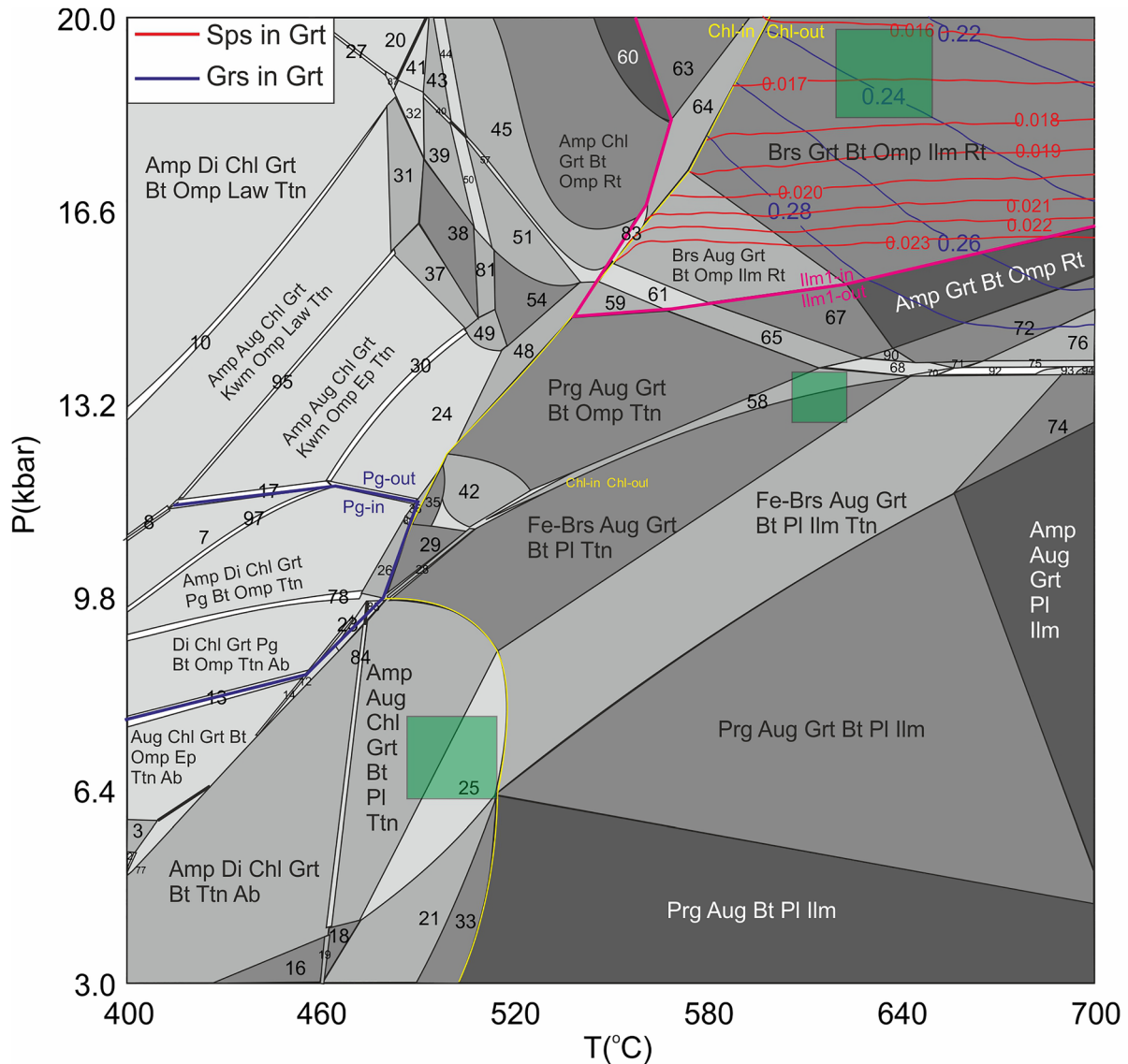


Fig. 7 (continued)

augite (Jd_{2-9}). Amphibole shows a wide compositional range (Fig. S1, Table S2). Amphibole inclusions in garnet are pargasite, ferro-pargasite with 18–24 mol% glaucophane component. Inclusions in rutile are barroisite with 35 mol% glaucophane component. Matrix amphiboles that are in textural equilibrium with garnet, omphacite and rutile are barroisite,

magnesio-katophorite with 27–45 mol% glaucophane component. Matrix amphiboles that are associated with albite (An_{3-8}) and replacing garnet and omphacite are katophorite, magnesio-katophorite, taramite, magnesio-taramite, ferro-pargasite and edenite. Their glaucophane component ranges from 17 to 36 mol%. Amphibole associated with garnet,



- 2 Aug Chl Grt Bt Omp Ves Ttn Ab
- 3 Aug Chl Grt Bt Omp Ttn Ab
- 7 Amp Aug Chl Grt Kwmm Pg Omp Ttn
- 8 Mica Mica Aug Chl Grt Amp Omp Law Ttn
- 10 Amp Aug Chl Grt Mica Bt Omp Law Ttn
- 12 Amp Aug Chl Grt Bt Omp Ttn Ab
- 13 Aug Chl Grt Mica Bt Omp Ep Ttn Ab
- 14 Amp Aug Chl Grt Bt Omp Ep Ttn Ab
- 16 Amp Aug Chl Bt Ttn Ab
- 17 Mica Mica Aug Chl Grt Amp Omp Ep Ttn
- 18 Amp Aug Chl Bt Pl Ttn
- 19 Amp Aug Chl Bt Pl Ttn Ab
- 20 Amp Aug Chl Grt Bt Omp Law Rt
- 21 Amp Aug Chl Bt Pl Ilm Ttn
- 23 Amp Aug Chl Grt Mica Bt Ttn Ab
- 24 Amp Aug Chl Grt Bt Omp Ep Ttn
- 25 Amp Aug Chl Grt Bt Pl Ilm Ttn
- 26 Amp Aug Chl Grt Mica Bt Ttn
- 27 Amp Aug Chl Grt Bt Omp Law Ttn Rt
- 28 Amp Aug Grt Mica Bt Pl Ttn
- 29 Amp Aug Grt Mica Bt Ttn
- 30 Amp Aug Chl Grt Mica Bt Omp Ep Ttn
- 31 Amp Chl Grt Mica Omp Law Ttn

- 32 Amp Chl Grt Mica Omp Law Ttn Rt
- 33 Amp Aug Chl Bt Pl Ilm
- 35 Amp Aug Grt Bt Ep Ttn
- 36 Amp Aug Chl Grt Bt Ep Ttn
- 37 Amp Chl Grt Mica Omp Ep Ttn
- 38 Amp Chl Grt Mica Omp Ttn
- 39 Amp Chl Grt Mica Omp Ttn Rt
- 40 Amp Aug Chl Grt Mica Omp Ttn Rt
- 41 Amp Aug Chl Grt Mica Omp Law Rt
- 42 Amp Aug Grt Bt Omp Ep Ttn
- 43 Amp Aug Chl Grt Mica Omp Rt
- 44 Amp Aug Chl Grt Mica Bt Omp Rt
- 45 Amp Aug Chl Grt Bt Omp Rt
- 48 Amp Aug Chl Grt Bt Omp Ttn
- 49 Amp Chl Grt Bt Omp Ep Ttn
- 50 Amp Chl Grt Mica Bt Omp Ttn Rt
- 51 Amp Chl Grt Bt Omp Ttn Rt
- 54 Amp Chl Grt Bt Omp Ttn
- 57 Amp Aug Chl Grt Bt Omp Ttn Rt
- 58 Amp Aug Grt Bt Pl Omp Ttn
- 59 Amp Aug Grt Bt Omp Ilm Ttn
- 60 Chl Grt Bt Omp Rt
- 61 Amp Aug Grt Bt Omp Ilm Ttn Rt

- 63 Chl Grt Bt Omp Ilm Rt
- 64 Amp Chl Grt Bt Omp Ilm Rt
- 65 Amp Aug Grt Bt Omp Ttn Rt
- 67 Amp Aug Grt Bt Omp Rt
- 68 Amp Aug Grt Bt Pl Omp Ttn Rt
- 70 Amp Aug Grt Bt Pl Ilm Ttn Rt
- 71 Amp Grt Bt Pl Omp Ttn Rt
- 72 Amp Grt Bt Pl Omp Rt
- 74 Amp Aug Grt Pl Ilm Ttn
- 75 Amp Grt Bt Pl Omp Ilm Ttn Rt
- 76 Amp Grt Bt Pl Omp Ilm Rt
- 77 Amp Aug Chl Grt Bt Omp Ves Ttn Ab
- 78 Amp Aug Chl Grt Mica Bt Omp Ttn Ab
- 81 Amp Chl Grt Mica Bt Omp Ttn
- 83 Amp Aug Chl Grt Bt Omp Ilm Rt
- 84 Amp Aug Chl Grt Bt Pl Ttn Ab
- 85 Amp Aug Chl Grt Mica Bt Pl Ttn
- 87 Amp Chl Grt Bt Omp Law Ttn Rt
- 90 Amp Aug Grt Bt Pl Omp Rt
- 91 Amp Aug Grt Bt Pl Ttn Rt
- 92 Amp Aug Grt Bt Pl Omp Ilm Ttn Rt
- 93 Amp Aug Grt Bt Pl Omp Ilm Ttn
- 94 Amp Aug Grt Pl Omp Ilm Ttn
- 95 Amp Aug Chl Grt Mica Omp Ep Law Ttn
- 97 Mica Mica Aug Chl Grt Amp Bt Omp Ttn
- 98 Amp Chl Grt Mica Bt Omp Law Ttn

Fig. 8 P–T pseudosection (H_2O saturated) for the eclogite SM-5 sample (SiO_2 : 46.04; TiO_2 : 2.88; Al_2O_3 : 14.62; FeO : 14.26; MnO : 0.26; MgO : 7.06; CaO : 10.42; Na_2O : 3.67; K_2O : 0.12; oxides in wt%). Compositional isopleths –calculated with WERAMI– for spessartine and grossular content in garnet are given in red, and blue lines, respectively (within the field Brs–Grt–Bt–Omp–Ilm–Rt). Rectangulars correspond to the estimated local-equilibrium P–T conditions. The yellow, purple, and dark blue continued lines correspond to the stability fields of chlorite, ilmenite-1, and paragonite, respectively. Light to dark grey indicate low-to high- variance fields. Thick black lines correspond to univariant reactions

albite and quartz is also magnesio-taramite. This association replaces paragonite and probably omphacite (Fig. 7c, d). Amphibole inclusions in omphacite are pargasite with 23 mol% glaucophane component. This amphibole replaces paragonite and omphacite and is associated with plagioclase (An_{15}) (Fig. 7e). Amphibole symplectically intergrown with oligoclase (An_{13-17}) is magnesio-hornblende or actinolite. Paragonite included in garnet is richer in margarite component (14–27 mol%) compared to paragonite inclusions in omphacite (2–3 mol%) (Table S2). The Fe_2O_3 content in clinozoisite ranges from 8.1 to 8.5 wt%.

The Melissochori/Svoula formation in the W-CRZ (metapelite Ph-1G)

We also investigated a metapelite of the *Melissochori/Svoula formation (sample Ph-1G)* to test if that the W-CRZ underwent a prograde HP metamorphism along a low geothermal gradient like the intercalations in the VOC. Major phases are phengite, chlorite, albite, quartz, minor epidote, titanite and hematite and accessories tourmaline, ilmenite, rutile. Phengite (Si ranges from 6.61 to 6.89 a.p.f.u.) is rich in iron. Total iron (expressed as FeO) ranges from 4.16 to 5.19 and MgO from 2.09 to 2.82 (Table S3). Petrography, textures and mineral compositions of sample Ph-1G are given in supplementary and shown in Fig. S2 and Table S3.

Discussion

P–T path of eclogites and metapelites of the intercalations in the VOC

Two P–T pseudosections (Figs. 8, 9) were calculated in the system SiO_2 – TiO_2 – Al_2O_3 – MgO – MnO – FeO – CaO – Na_2O – K_2O – H_2O (with pure H_2O in excess), employing Perple_X software (ver. 6.8.9; 2020, Connolly 1990, 2005, 2009; see Supplementary material).

The eclogite SM-5 and the metapelite B-5 both preserve mineral assemblages equilibrated near the peak of metamorphism. Hence, the constructed pseudosections are used to evaluate the eclogitic conditions. As such, the compositions

of characteristic minerals formed at or near the peak of metamorphism like garnet and/or omphacite are used as proxies for the peak conditions. Furthermore, the retrograde metamorphism is associated with local re-equilibration of the mineral assemblages during exhumation. Hence, this influences the textures or/and the chemistry of phases in close contact like in the case of the coexisting phases kyanite, phengite, chlorite, and staurolite. Also, the composition which effectively reacts and equilibrates the rock volume is in the mineral scale and may differ from domain to domain of the analysed thin sections. Due to that, we suggest that the calculated pseudosections can be regarded as good proxies for determining the peak conditions, while the estimated post-peak conditions should be regarded as tentative.

Eclogite SM-5

Based on mineral chemistry, textural relationships and calculated assemblages of the eclogite from the Nea-Roda area (Fig. 2; SM-5) a P–T history can be defined for: (i) the peak P–T conditions, and (ii) post-peak stage of decompression through epidote–amphibolite and amphibolite facies metamorphism. The prograde P–T path can be tentatively discussed, based on the inclusions of clinozoisite/epidote, paragonite, ferro-pargasite and rutile in garnet and omphacite, and inclusions of barroisite in garnet, omphacite and rutile (Fig. 6a–e). The presence of epidote, paragonite, barroisite and ferro-pargasite (rich in glaucophane component) inclusions in garnet and omphacite, and the absence of Na-amphiboles indicate that the prograde PT-path traversed the epidote–amphibolite facies field and entered the eclogite facies field (fields of metamorphic facies according to Oh and Liou 1998).

Texturally, the mineral assemblage Grt + Omp + Qz + Rt + Brs records the eclogite facies metamorphism. The calculated P–T pseudosection is used to estimate the peak conditions. The isopleths for garnet, were superimposed on the P–T pseudosection. The intersection of the grossular ($24 \pm 2\%$) and spessartine ($1.7 \pm 0.1\%$) isopleths, along with the sodic-calcic amphibole chemistry, which all match the observed compositions of garnet and amphibole indicate P 1.91 ± 0.08 GPa and T 640 ± 25 °C (Fig. 8). As such, the calculated conditions within the Grt + Omp + Brs + Bt + Ilm + Rt field are in accordance with the observed data. The peak P–T conditions for the eclogite facies stage suggest a mean geothermal gradient of ~ 9 – 11 °C/km during subduction.

In early stages of decompression, eclogitic omphacite (Jd_{49}) is first decomposed to Na-poorer omphacite (Jd_{33}) and albite. Then, garnet and omphacite have been replaced by kelyphitic amphibole (barroisite, magnesio-katophorite, ferro-pargasite, ferro-edenite), clinozoisite and albite (Fig. 7a, b, e) indicating decompression through the field of

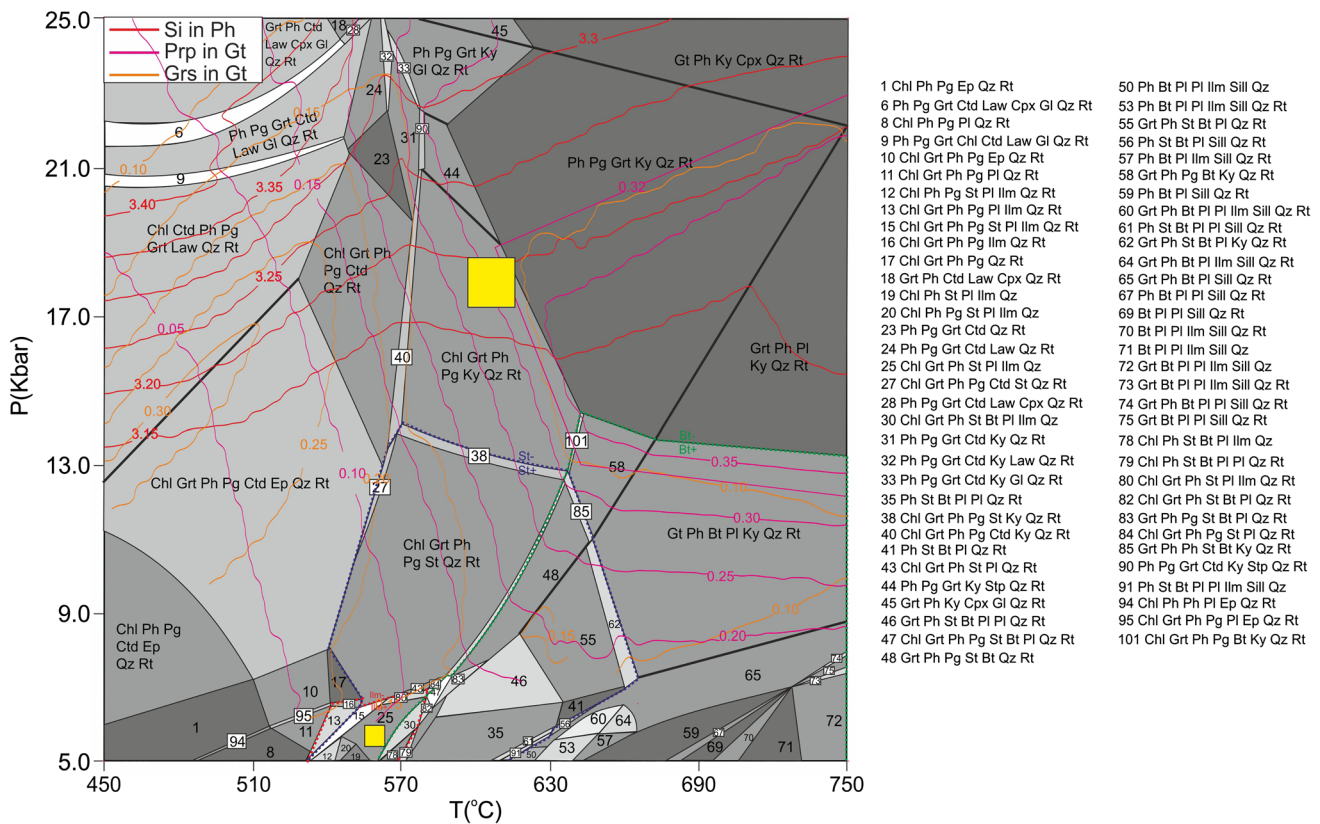


Fig. 9 P–T pseudosection (H_2O saturated) for the metapelite B-5 sample (SiO_2 : 57.53; TiO_2 : 0.91; Al_2O_3 : 20.9; FeO : 6.20; MnO : 0.06; MgO : 2.62; CaO : 0.88; Na_2O : 0.80; K_2O : 3.00; oxides in wt%). Rectangulars correspond to the estimated local-equilibrium P–T

conditions. The green, blue, and red dashed lines correspond to the stability fields of biotite, staurolite, and ilmenite, respectively. Field coloring and thick black lines as in Fig. 8

the epidote–amphibolite facies. The decompression path is further characterized by the coexistence of ferro-pargasite, clinozoisite and albite replacing garnet and omphacite (Fig. 7f). Hence, in the calculated pseudosection, this is indicated by the narrow Amp + Aug + Grt + Bt + Omp + Ttn + Pl field (Fig. 8) at $P \sim 13.2$ GPa where the amphibole and plagioclase chemistry match the observed pargasitic amphibole and albitic plagioclase, respectively. In later stages, during continuing decompression, the presence of chlorite, and ilmenite-2 + titanite (Fig. 7k, l) indicates stability within the Amp + Aug + Chl + Grt + Bt + Pl + Ttn + Ilm field at $P \sim 0.64 \pm 0.15$ GPa and $T \sim 490 \pm 25$ °C (Fig. 8).

Metapelite B-5

The observed compositional—bell-shaped—zoning of garnet indicates prograde formation as suggested by the calculated almandine, grossular, and pyrope isopleths (Figs. 5, 9). As such, the simultaneous increase in pyrope and decrease in grossular contents are only consistent with a path associated with a continued increase either of pressure and temperature

along a cold geothermal gradient, or temperature only but still at high- $P > 1.6$ GPa (Fig. 9).

The presence of ilmenite inclusions in the Ca-rich garnet core and rutile inclusions in garnet rim (Fig. 3c) indicate that garnet growth had already started during the early stages of the prograde P–T path before entering the stability field of rutile. We attempted to model the ilmenite-rutile transition using the bulk-composition of sample B-5. Starting at low-T/P, however, even for P as low as 1 kbar and T 350 °C, it was not possible to stabilize ilmenite along a prograde path. In contrast, the pseudosections calculated by Kydonakis et al. (2015) for the Volvi area, which recorded similar P–T conditions, show ilmenite at $P < 1.1$ GPa and $T < 570$ °C. Consequently, it is possible that a bulk-composition effect controls the ilmenite formation during prograde metamorphism.

In the garnet-kyanite-staurolite mica schist B-5 of the Nea-Roda area (Fig. 2) the peak mineral assemblage is Chl + Grt + Ky + Ph + Qz + Rt + Pg documenting P–T conditions at $\sim 1.7 \pm 1$ GPa and 580–600 °C within the high variance field of garnet-kyanite-phengite-rutile-paragonite-chlorite (Fig. 9), based on observed textures and composition of

garnet and phengite. The predicted paragonite is stable at the peak conditions experienced by our rock. However, our inability to observe it in our thin sections is associated with its replacement by plagioclase during decompression. Thus, the inferred P–T conditions are similar to those constrained from the neighboring eclogite SM-5 (Fig. 8).

A decompression stage in the P–T evolution is reflected in the textural relationships of chlorite-staurolite-biotite, and in chemistry of staurolite suggesting a good constraint at mid-P/T conditions. The latter was influenced by the presence of Zn; in our studied sample the relatively high Zn-content, suggests a displacement of the stability field of staurolite toward lower temperatures. As such, the stability fields of staurolite-chlorite-biotite have been traversed as suggested by the textural relationships and verified by the calculated pseudosection. This, however, should be regarded as tentative (Figs. 4b–e, 9). In particular, when the decompression path entered the stability field of staurolite-chlorite-muscovite, kyanite has been replaced, according to the following reaction:

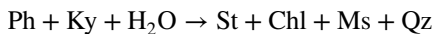


(Fig. 4b, c). In contrast, the decompression path traversed the stability field of biotite at T higher than that of the chlorite field (Fig. S3). Staurolite and biotite may have co-formed at the expense of garnet, chlorite and muscovite in accordance with the petrographic data (staurolite associated with resorbed garnet; Fig. 4e). Furthermore, during decompression, a second ilmenite (Ilm-2) associated with chlorite, staurolite and muscovite replaced the rutile. Ilm-2 shows shape-preferred orientation parallel to that of the inclusions of rutile in kyanite (Fig. 4b, c), suggesting that Ilm-2 replaced rutile. Hence, the associated staurolite was formed either within the stability field of ilmenite in agreement with our petrographic observations or preceded ilmenite formation in agreement with the calculated pseudosection. As such, the mis-match between petrographic (co-occurrence of staurolite and ilmenite) observations and calculated pseudosection (staurolite fractionated earlier compared to ilmenite) may be due to kinetic reasons, limited access of aqueous fluid, or/and local changes in effective bulk-composition; since the retrograde history should be regarded as tentative we do not further comment on any of these factors.

P–T histories of the tectonic intercalations in VOC, PCMA and W-CRZ versus P–T history of the VOC

Our results indicate that the metamorphic history of the tectonic intercalations within the eastern VOC—consisting of metapelites, metabasites, meta-rhyolites, quartzites and marbles (Fig. 2)—is more similar to that of the PCMA and W-CRZ than to that of the VOC.

The VOC consists of pre-Alpine continental crust (Himmerkus et al. 2009a; Peytcheva et al. 2015) that underwent three metamorphic events. The first one was HP/UHP-HT with P–T conditions of 3.0–3.5 GPa and 700–750 °C at the UHP stage, followed by partial melting and migmatite formation, associated with a temperature increase to 800–850 °C (at ~1.1 GPa), during decompression (Janak et al. 2011; Peytcheva et al. 2015; Mposkos et al. 2021). It was Variscan constrained by the 334 Ma Lu–Hf garnet-whole rock ages of kyanite eclogites (Trapp et al. 2020) and 321 Ma, U–Pb zircon ages of neosomes from migmatitic orthogneisses (Peytcheva et al. 2015). The second metamorphic cycle was of LP-HT accompanied with partial melting and migmatite formation within the stability field of sillimanite, cordierite and K-feldspar with peak P–T conditions 0.44 ± 0.04 GPa and 745 ± 30 °C (Mposkos et al. 2021). It is associated with Permo-Triassic rifting and related Triassic A-type bimodal magmatic intrusions (U–Pb magmatic zircons 240–222 Ma) (Himmerkus et al. 2009b; Bonev et al. 2019a and references therein). The LA-ICP-MS U–Th–Pb monazite ages from a garnet-kyanite metapelite is in the range of 310–230 Ma with a dominant cluster of 257.4 ± 1.1 Ma. Matrix monazites decomposed at their outer parts into a corona made of apatite-allanite-epidote yielded at their rims ages of 132.5 ± 0.3 Ma (Kydonakis et al. 2016). We interpret the Triassic monazite ages in the metapelite to record roughly the LP-HT metamorphic event in VOC. The third metamorphic cycle was MHP with increasing grade of metamorphism from the SW to NE and peak P–T conditions 1.05 ± 0.08 GPa and 690 ± 30 °C recorded in metapelites.

Dixon and Dimitriadis (1987) report temperatures of 700–750 °C obtained with garnet-hornblende thermometry in garnet amphibolites from the Triassic mafic Volvi complex. The MHP metamorphism occurred in late Jurassic–early Cretaceous (Mposkos et al. 2021). A phlogopite of a Triassic phengite-bearing meta-granitoid yielded an ^{40}Ar – ^{39}Ar age of c. 136 Ma (de Wet et al. 1989). The c. 132 Ma monazite-rim ages from the garnet-kyanite metapelite are interpreted by Kydonakis et al (2016) to date the amphibolite facies overprint of the eclogite facies metamorphism recorded in the intercalations during decompression. They assume that in late Jurassic–early Cretaceous the VOC and the intercalations of W-CRZ in VOC are metamorphosed at eclogite facies P–T conditions as a coherent unit. ^{40}Ar – ^{39}Ar cooling ages of white micas range from 123 to 127 Ma (Kydonakis et al. 2016). We interpret the c.132 Ma U–Th–Pb ages of the monazite-rims and ^{40}Ar – ^{39}Ar ages of phlogopite and white micas as roughly dating the time of youngest MHP metamorphic event in VOC.

By contrast, the tectonic intercalations of W-CRZ in the eastern VOC show only one HP/LT metamorphic event, like the PCMA and the W-CRZ. Our petrological data from eclogite SM-5 and metapelite B-5 record P–T conditions

of ~ 1.9 GPa/640 °C and ~ 1.7 GPa/590 °C respectively. Also, eclogite facies P–T conditions of ~ 1.9 GPa/520 °C are documented by Kydonakis et al. (2015) in chloritoid bearing garnet-staurolite schists in the areas north and south of Volvi-lake (Fig. 2). This indicates that the prograde P–T path of the intercalations followed a lower geothermal gradient (~ 9–11 °C/km) than that of the MHP metamorphism of the VOC (~ 17.7 °C/km; Mposkos et al. 2021). The sedimentary protoliths of the metapelites were deposited from Triassic to middle-Jurassic (Kockel et al. 1977; Dixon and Dimitriadis 1984; Sakellariou and Dürr 1993; Kydonakis et al. 2015) setting the lower time limit in the late Jurassic–early Cretaceous for the age of HP metamorphism in the intercalations.

Similar to the tectonic intercalations in eastern VOC, the PCMA and W-CRZ show only one HP/LT metamorphic event but at lower pressures and temperatures of ~ 0.6–0.9 GPa at 300–400 °C (Michard et al. 1994; Baroz et al. 1987) or 0.8 GPa/550 °C (Kydonakis et al. 2015). The phyllite of the Melissochori/Svoula formation (sample Ph-1G; Fig. 2) of the W-CRZ, investigated in this study, has the mineral assemblage Ph + Chl + Ab + Ep + Qz + Ttn + Ti-Hem typical for the greenschist facies. High pressures are indicated by high-Si phengite (Si = 6.89 a.p.f.u.). For temperatures of 300–400 °C this corresponds to minimum pressures of 0.8–0.9 GPa (Massonne and Schreyer 1987). In the W-CRZ, ⁴⁰Ar–³⁹Ar white mica ages of c. 124–125 Ma are interpreted by Kydonakis et al. (2016) as approximating the age of the HP/LT metamorphism. This suggests that the intercalations in the eastern VOC are part of the same coherent subducted unit as the W-CRZ but represent a deeper segment.

East Vardar/Axios ophiolite: oceanic crust between the VOC complex and southern European margin

The East Vardar/Axios ophiolites (Peonias ophiolites in Greek area) consist of mid-ocean ridge basalt (MORB) and island arc tholeiite (IAT) as shown by their geochemical signatures (Mussallam and Jung 1986; Bébien et al. 1986, 1987; Zachariadis 2007; Bonev et al. 2015b and references therein). U–Pb zircon ages at ~ 169–149 Ma indicate formation of the ophiolites in the middle to late Jurassic (Anders et al. 2005; Zachariadis 2007; Božović et al. 2013; Bonev et al. 2015b). Fossiliferous Tithonian conglomerates and Kimmeridgian to Berriasian–early Valanginian reefal limestones cover the ophiolites (Mercier 1968; Kockel et al. 1977; Bonev et al. 2015b; Ivanova et al. 2015), providing a minimum age limit of formation and emplacement of the ophiolites. They have been interpreted as formed in a short living oceanic basin along a dextral wrench zone in a back-arc setting above the north dipping subduction beneath the PCMA (Bébien et al. 1986; Brown and Robertson 2003). Emplacement of the ophiolites is considered to be associated

with multiple north dipping subduction zones within the middle-late Jurassic Paikon–Chortiatia arc/back-arc system (Zachariadis 2007; Božović et al. 2013), or to a south dipping subduction (Jahn-Awe et al. 2010; Froitzheim et al. 2014; Bonev et al. 2015b and references therein).

Location of E-Vardar/Axios ocean

The E-Vardar (Peonias) ophiolites are associated with tectonic slivers of continental crustal rocks (Pigi and Karathodoros area; Zachariadou and Dimitriadis 1994; Fig. 2). We interpret these slivers as continental crust originating from the VOC. Similar to the VOC, they typically show LP-HT metamorphism, migmatitic fabrics and deformation during decompression. The mineral assemblages of metapelites in the slivers (Grt + Bt + Sil + Crd + Kfs + Pl + Qz + Spl(Hc) + Ilm indicate P–T conditions of $P < 0.4$ GPa and $T \sim 750$ °C (Zachariadou and Dimitriadis 1994), which are similar to those in the metapelites of the central and eastern VOC (Dixon and Dimitriadis 1987; Mposkos et al. 2021). Also, the U–Pb SHRIMP ages of zircon cores of the slivers fall in the range of those of the VOC, e.g. zircon U–Pb ages of the migmatitic cordierite granite of the Karathodoros sliver are c. 284, 430, 460 and 520 Ma (Anders et al. 2005). In the present state, metapelites and migmatites analogous to the slivers of the Karathodoros and Pigi areas are not present in the western VOC adjacent to the E-Vardar/Axios ophiolites (Zachariadou and Dimitriadis 1994; Dixon and Dimitriadis 1987; Mposkos et al. 2021). Hence, the original location of the E-Vardar/Axios oceanic basin must have been to the NE of VOC (see more details in Supplementary).

Plate tectonic reconstruction in the broad area

Succession of Alpine tectonic events

Based on the PT-data of the VOC (Mposkos et al. 2021) and the newly presented PT-data of the W-CRZ (this study; see also supplementary info), a new model for the late Jurassic–early Cretaceous geodynamic evolution of the eastern Hellenides is proposed (Fig. 10):

- A. The LP-HT metamorphism in the tectonic slivers in E-Vardar ophiolite zone (Peonias zone) and the VOC is interpreted to reflect Triassic extension and rifting of the European continental margin, in agreement with previous interpretations (Zachariadou and Dimitriadis 1994; Mposkos et al. 2021) (Fig. 10a). Triassic extension is also indicated by the volcanic activity in the Early–Middle Triassic Pirghoto formation of W-CRZ and the magmatic intrusions in VOC and in southern Sakar–Strandja Massif (Himmerkus et al. 2009b; Asvesta and Dimitriadis 2010; Bonev et al. 2019a)(Fig. 10a). Rifting

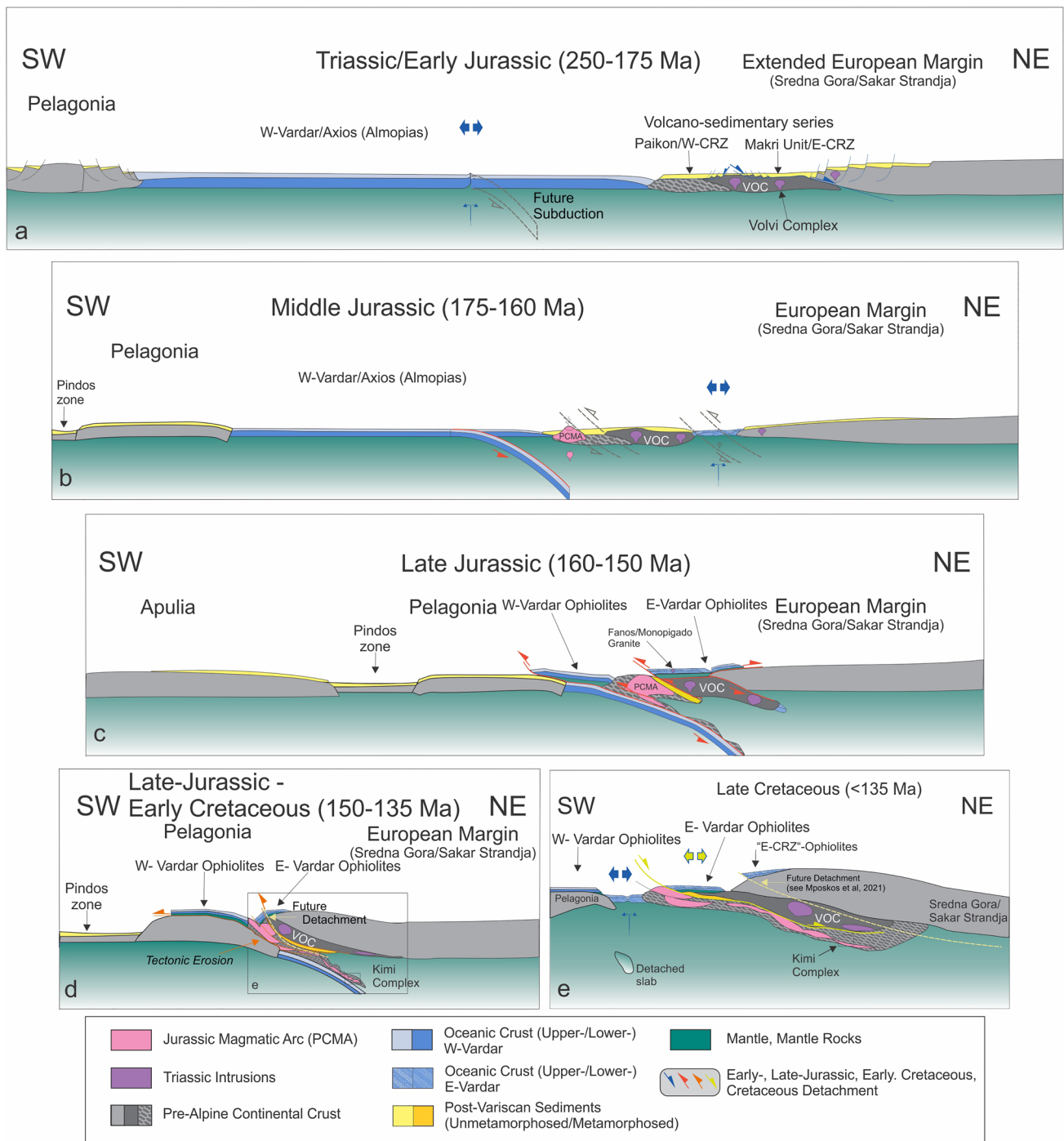


Fig. 10 Reconstruction of the Triassic-early Cretaceous plate tectonic evolution of the Eastern Hellenides. See text for explanation

started in the continental crust (Fig. 10a). The Carboniferous-Permian (~ 330–290 Ma) prominent population of detrital zircon ages in meta-sandstones from the late Triassic-middle Jurassic Melissochori Formation in W-CRZ and the Carboniferous-Permian (~ 310–290 Ma) and Triassic (~ 240 Ma) detrital zircons from the pre-Cretaceous Makri unit in E-CRZ (Meinhold and Kostopoulos 2013)

suggest significant input of Carboniferous-Permian igneous rocks in the sandstones of both units. Supply of detrital grains from orthogneisses of VOC can be excluded since the majority of the orthogneisses in VOC have Ordovician–Silurian protolith ages (Himmerkus et al. 2009a; Peytcheva et al. 2015 and references therein). Orthogneisses from the Sakar-Strand Massif

are the closest possible sources to supply detrital material in Melissochori Formation and Makri unit, since Carboniferous–Permian and Triassic granitoids are present in this Massif (Bonev et al. 2019b, c and references therein). In the E-Vardar/Axios area, rifting started in the continental crust (Fig. 10a).

- B. In the middle-late Jurassic, the PCMA is interpreted to have formed as a result of NE-directed subduction of the W-Vardar/Axios Ocean (Almopias Ocean)— separating the Pelagonia continental margin from Europe—beneath the South European plate margin (Fig. 10b). Above the subduction zone, at the South-European plate margin, a magmatic arc formed (PCMA) and an oceanic basin (E-Vardar/Axios Ocean) separating the eastern-VOC from the South-European continental margin (Sredna Gora and Sakar–Strandja Massif). In North Macedonia and Greece back-arc spreading was separated from the drifted continental fragment (VOC, Fig. 10b). In West Carpathian, arc and back-arc basin are developed in oceanic realm (Gallhofer et al. 2017; Boev et al. 2018).
- C. In the late Jurassic in the W-Vardar/Axios Ocean the NE directed subduction continued. Following the intra-oceanic subduction (Bortolotti et al. 2012; Schenker 2013), detachment and obduction of the W-Vardar/Axios ophiolites on the Pelagonian zone occurred (Kiliyas et al. 2010; Papanikolaou 2009; Schenker 2013; Brown and Robertson 2003). Further, in the E-Vardar/Axios area, extension switched to compression, thus causing subduction and closing of the back-arc marginal basin and obduction of the E-Vardar (Peonias) ophiolites over the VOC and back thrusting over the Sakar–Strandja continental margin (Sunal et al. 2011) (Fig. 10c). At the same period, the arc magmatic activity has been shifted toward NE as indicated by the presence of Monopigadon and Fanos granites, and Sithonia rhyolite which intruded E-Vardar ophiolites at c. 159, 158, and 149 Ma, respectively (Anders et al. 2005; Meinhold et al. 2009; Bonev et al. 2015b) (Fig. 10b, c).
- D. With continuing convergence, the Pelagonia continental margin entered the subduction zone and collided with PCMA triggering subduction of the latter and the W-CRZ (e.g. Chementa et al. 2001) (Fig. 10d). Subduction of Pelagonia is clearly associated with a metamorphic event recorded at 1.1 GPa/500 °C (Mposkos et al. 2001; Mposkos and Krohe 2004; Schenker 2013). Additionally to that, the subduction of the PCMA, W-CRZ and VOC is associated with the late Jurassic–early Cretaceous HP/LT metamorphism in PCMA and W-CRZ, the MHP metamorphism in VOC and the eclogite facies metamorphism in tectonic intercalations of W-CRZ in eastern VOC (Baroz et al. 1987; Michard et al. 1994; Kydonakis et al. 2015; Mposkos et al. 2021; this work). In VOC, the relatively high geothermal gradient during

the prograde path and peak conditions (~ 17.7 °C/km for pressure of 1.05 GPa and temperature of 690 °C; see Fig. 21 in Mposkos et al. 2021) is characteristic for subduction into a warmer environment, e.g. beneath a young and, hence, warm oceanic plate (e.g. obducted E-Vardar/Axios oceanic lithosphere). A NE-ward increase of metamorphic grade of the MHP and HP metamorphism in VOC and W-CRZ indicates NE-directed polarity of this subduction (Mposkos et al. 2021; Kydonakis et al. 2015; this work, Fig. 10d).

- E. During early Cretaceous exhumation of the subducted Pelagonia continental margin, the PCMA, W-CRZ and VOC followed the slab roll-back and slab detachment (Fig. 10e). In Pelagonia zone metamorphic zircon rim ages of c. 130–110 Ma and $^{40}\text{Ar}/^{39}\text{Ar}$ mica cooling ages of c. 116–100 Ma (Schenker 2013 and references therein) constrain various stages of decompression. In W-CRZ $^{40}\text{Ar}/^{39}\text{Ar}$ white mica cooling ages of c. 125–119 constrain a stage of decompression. In VOC U-Th-Pb monazite ages of c. 132 Ma and $^{40}\text{Ar}/^{39}\text{Ar}$ white mica cooling ages of c. 127–124 Ma in western VOC and 104–95 Ma in eastern VOC, and 100–97 Ma in the tectonic intercalations of W-CRZ in eastern VOC (Kydonakis et al. 2016) constrain various stages of decompression and cooling.

In the overriding ophiolites, extension and subsidence started in latest Jurassic, while at the same time continental subduction continued. Tithonian conglomerates with ophiolitic detritus and Tithonian-early Cretaceous (Berriasian–early Valanginian) shallow-water limestones cover the E-Vardar ophiolites (e. g. Mercier 1968; Kockel et al. 1977; Ivanova et al. 2015) suggesting starting of extension and subsidence in this area. In the western margin of the W-Vardar ophiolite zone (Almopias zone) extension and subsidence are registered by late Jurassic–early Cretaceous neritic carbonate and terrigenous clastic deposits and intermediate–silicic magmatism. New oceanic crust (Meglenitsa Ophiolite) formed in eastern Almopias zone during early Cretaceous (Sharp and Robertson 2006 and references therein).

In the present state, unmetamorphosed ophiolites (and associated sediments) of the E-Vardar/Axios zone immediately overlie the HP-metamorphic rocks of the W-CRZ and the PCMA along narrow tectonic contacts. Hence, tectonic movements postdating subduction must have emplaced these units against each other. Estimating from the metamorphic pressure of the HP metamorphism, at least 30 km thick section of the crust has been cut out between the ophiolites and the underlying units. In our schematic (Fig. 10e), we consider the basal contact of the E-Vardar/Axios ophiolite zone as a large-scale system of extensional detachment faults extending from the Paikon area to the east RMD, formed in

the late Cretaceous and early Tertiary (Fig. 10e). Cenomanian transgression indicates that the PCMA was lifted to the surface already at ~100 Ma in the Paikon area (Mercier 1968).

Eastern continuation of the W-CRZ and PCMA into the central and eastern RMD

The PCMA, the W-CRZ and the tectonic intercalations of W-CRZ in eastern VOC possibly continue farther to the east into the central and east RMD (Fig. 10d,e). There, this structural event is likely represented by Segments I and II (i.e. Kimi, and Sidironero complexes; Fig. 1). Both segments also consist of meta-pelites, meta-psammites and meta-carbonates as well as orthogneisses and amphibolites. They are possible equivalents of the volcano-sedimentary succession of the W-CRZ and the Jurassic PCMA complexes, respectively. Like in the PCMA, orthogneisses and amphibolites of these segments also show middle to late Jurassic protolith ages (e.g. von Quadt et al. 2009; Turpaud and Reischman 2010; Bosse et al. 2009; Liati et al. 2011; Froitzheim et al. 2014; Bonev et al. 2015a; Pleuger et al. 2020). This is an important difference to the VOC, which lacks orthogneisses and amphibolites with Jurassic protolith ages. In the RMD, these rocks were subducted to greater depths.

In segments I and II, the late Jurassic–early Cretaceous metamorphism indicates HP-HT conditions. Also, decompression occurred at higher temperatures leading to partial melting, melt segregation, melt intrusion, and migmatization (Mposkos and Krohe 2000, 2006; Liati et al. 2011; Bauer et al. 2007; Georgieva et al. 2010; Bosse et al. 2009; Kirchenbaur et al. 2012; Wawrzenitz et al. 2015). Considering the comparable P–T paths observed in PCMA, W-CRZ, the intercalation of W-CRZ in eastern VOC, and Segment I and II of the central and eastern RMD, all attributed to late Jurassic–early Cretaceous HP metamorphism, we propose their amalgamation into a single terrane, the “Eohellenic HP-Belt”.

In this reconstruction (Fig. 10c–e), the PCMA, W-CRZ and Segments I and II of the RMD are part of the same NE plunging subducted plate. While the PCMA and W-CRZ have been subducted to shallower depths, segments I and II of the RMD represent the deeper parts of this plate. Jurassic NE subduction of Segments I and II is also proposed by Krenn et al. (2010) and Kydonakis et al. (2015). The NE-direction of subduction proposed in this study is consistent with the tectonic reconstruction of Schmid et al. (2020) placing the W-CRZ underneath the VOC (Fig. 11 in Schmid et al. 2020).

It should be noted that HP- metamorphism in the structurally lowermost segment III is unrelated to the late Jurassic–early Cretaceous subduction event described here. HP metamorphism of segment III occurred during the late

Cretaceous-early Tertiary and is associated with subduction and closure of the Neo-Tethys and collision of Apulia with Europe (Dinter 1998; Miladinova et al. 2018; Jahn-Ave et al. 2010, 2012; Froitzheim et al. 2014).

Conclusion

Considering literature data alongside our new petrologic work, we newly define the Eohellenic HP belt, consisting of pre-Alpine basement (VOC), continental volcano-sedimentary formations (W-CRZ) and a Jurassic magmatic arc (PCMA). We suggest that the Eohellenic HP-Belt was subducted in late Jurassic- early Cretaceous beneath the European plate margin consisting of the Sakar–Strandja Massif, the continental European margin sediments, oceanic sediments and ophiolites. Subduction occurred when the Pelagonia continental margin entered the subduction zone triggering (1) the subduction of the Eohellenic HP-Belt and (2) obduction of the E-Vardar (Peonias) ophiolites over the Eohellenic HP-Belt along with back-thrusting over the southern margin of the Sakar–Strandja Massif.

The VOC has been accreted shortly before, beneath a hot oceanic lithosphere (as is indicated by its high geothermal gradient during the peak of the MHP metamorphism) of the middle-late Jurassic E-Vardar/Axios back-arc oceanic basin that separated the VOC from the southern European margin. The E-Vardar/Axios oceanic basin was, thus, originally situated to the NE of the VOC.

NE subduction of the Eohellenic HP-Belt is in agreement with a northeastward increase in the metamorphic grade of the late Jurassic–early Cretaceous HP metamorphism in PCMA, W-CRZ including the intercalations of the W-CRZ in eastern VOC and segment I and II in RMD. In this interpretation segment I and II of the RMD, which similarly comprise pre-Alpine basement rocks (with protolith ages similar to VOC, Bonev et al. 2013 and references therein), meta-volcano-sedimentary sequences, Jurassic oceanic crust and rocks of the Jurassic magmatic arc, are the more deeply subducted parts of the Eohellenic HP-Belt farther to the northeast. In future, improved knowledge of the geodynamic evolution of the eastern Hellenides and additional computational models will help us to put geological constraints on a broad area of the Eastern Mediterranean.

Supplementary Information The online version contains supplementary material available at <https://doi.org/10.1007/s00531-023-02368-5>.

Acknowledgements The reviewers Nikolay Bonev, Thorsten Nagel and the topic editor Nikolaus Froitzheim are gratefully appreciated for comments that helped to significantly improve an earlier version of the manuscript. The editor-in-Chief, Ulrich Riller, is also thanked for his review and the fruitful comments.

Funding Open access funding provided by HEAL-Link Greece.

Data availability The authors confirm that the data supporting the findings of this study are available as Supplementary material.

Declarations

Conflict of interest The authors declare that they have no known competing financial interests or personal relationships that could have appeared to influence the work reported in this paper.

Open Access This article is licensed under a Creative Commons Attribution 4.0 International License, which permits use, sharing, adaptation, distribution and reproduction in any medium or format, as long as you give appropriate credit to the original author(s) and the source, provide a link to the Creative Commons licence, and indicate if changes were made. The images or other third party material in this article are included in the article's Creative Commons licence, unless indicated otherwise in a credit line to the material. If material is not included in the article's Creative Commons licence and your intended use is not permitted by statutory regulation or exceeds the permitted use, you will need to obtain permission directly from the copyright holder. To view a copy of this licence, visit <http://creativecommons.org/licenses/by/4.0/>.

References

- Anders B, Reischmann T, Poller U, Kostopoulos D (2005) Age and origin of granitic rocks in the eastern Vardar Zone, Greece: new constraints on the evolution of the Internal Hellenides. *J Geol Soc (lond)* 162:857–870
- Asvesta A, Dimitriadis S (2010) Facies architecture of a Triassic rift-related silicic volcano-sedimentary succession in the Tethyan realm, Peonias subzone, Vardar (Axios) Zone, northern Greece: regional implications. *J Volc Geoth Res* 193:245–269
- Baroz F, Bébian J, Ikenne M (1987) An example of high-pressure low-temperature metamorphic rocks from an island arc: the Paikon Series (Innermost Hellenides, Greece). *J Metamorph Petrol* 5:509–527
- Bauer C, Rubatto D, Krenn K, Proyer A, Hoinkes G (2007) A zircon study from the Rhodope metamorphic complex, N-Greece: time record of a multistage evolution. *Lithos* 99:207–228
- Bébian J, Dubois R, Gauthier A (1986) Example of ensialic ophiolites emplaced in a wrench zone: innermost Hellenic ophiolite belt (Greek Macedonia). *Geology* 14:1016–1019
- Bébian J, Baroz J, Caperdi S, Venturelli G (1987) Magmatisme basique associées à l'ouverture d'un bassin marginal dans les Hellenides internes au Jurassique. *Ophioliti* 12:53–70
- Boev B, Cvetković V, Prelević D, Šarić K, Boev I (2018) East Vardar ophiolites revisited: a brief synthesis of geology and geochemical data. *Contrib Sect Nat Math Biotech Sci MASA* 39(1):51–68
- Bonev N, Ovtcharova-Schaltegger M, Moritz R, Marchev P, Ulianov A (2013) Peri-Gondwanan Ordovician crustal fragments in the high-grade basement of the Eastern Rhodope Massif, Bulgaria: evidence from U–Pb LA-ICP-MS zircon geochronology and geochemistry. *Geodin Acta* 26:207–229
- Bonev N, Marchev P, Moritz R, Collings D (2015a) Jurassic subduction zone tectonics of the Rhodope Massif in the Thrace region (NE Greece) as revealed by new U–Pb and ⁴⁰Ar/³⁹Ar geochronology of the Evros ophiolite and high-grade basement rocks. *Gondwana Res* 27(2):760–775
- Bonev N, Marchev P, Moritz R, Filipov P (2015b) Timing of igneous accretion, composition, and temporal relation of the Kassandra-Sithonia rift-spreading center within the eastern Vardar suture zone, Northern Greece: insights into Jurassic arc/back-arc systems evolution at the Eurasian plate margin. *Int J Earth Sci* 104(7):1837–1864
- Bonev N, Moritz R, Borisova M, Filipov P (2019a) Therma–Volvi–Gomati complex of the Serbo-Macedonian Massif, Northern Greece: a Middle Triassic continental margin ophiolite of Neotethyan origin. *J Geol Soc* 176(5):931–944
- Bonev N, Filipov P, Raicheva R, Moritz R (2019b) Triassic magmatism along the Maritsa river valley, Sakar–Strandzha Zone, Bulgaria. *Rev Bulg Geol Soc* 80:56–57
- Bonev N, Filipov P, Raicheva R, Moritz R (2019c) Timing and tectonic significance of Paleozoic magmatism in the Sakar unit of the Sakar-Strandzha Zone, SE Bulgaria. *Int Geol Rev* 61(16):1957–1979
- Bortolotti V, Chiari M, Marroni M, Pandolfi L, Principi G, Saccani E (2012) Geodynamic evolution of ophiolites from Albania and Greece (Dinaric–Hellenic belt): one, two, or more oceanic basins? *Int J Earth Sci* 102:783–811
- Bosse V, Boulvais P, Gautier P, Tiepolo M, Ruffet G, Devidal JL, Cherneva Z, Gerdjikov I, Paquette JL (2009) Fluid-induced disturbance of the monazite Th–Pb chronometer: in situ dating and element mapping in pegmatites from the Rhodope (Greece, Bulgaria). *Chem Geol* 261:286–302
- Božović M, Prelević D, Romer RL, Barth M, Van Den Bogaard P, Bonev B (2013) The Demir Kapija Ophiolite, Macedonia (FYROM): a snapshot of subduction initiation within a back-arc. *J Petrol* 54(7):1427–1453
- Brown SAM, Robertson AHF (2003) Sedimentary geology as a key to understanding the tectonic evolution of the Mesozoic-early Tertiary Paikon Massif, Vardar suture zone, N Greece. *Sed Geol* 160:179–212
- Brun J-P, Sokoutis D (2007) Kinematics of the Southern Rhodope core complex (North Greece). *Int J Earth Sci* 96(6):1079–1099
- Brun J-P, Sokoutis D (2018) Core complex segmentation in North Aegean, a dynamic view. *Tectonics* 37:1797–1830. <https://doi.org/10.1029/2017TC004939>
- Burg J-P (2012) Rhodope: From Mesozoic convergence to Cenozoic extension. Review of petro-structural data in the geochronological frame. *J Virtual Explor.* <https://doi.org/10.3809/jvirtex.2011.00270>
- Chemenda AI, Hurpin D, Tang J-C, Stephan J-F, Buffet G (2001) Impact of arc-continent collision on the conditions of burial and exhumation of UHP/LT rocks: experimental and numerical modelling. *Tectonophysics* 342:137–161
- Connolly JAD (1990) Multi-variable phase diagrams: an algorithm based on generalized thermodynamics. *Am J Sci* 290:666–718
- Connolly JAD (2005) Computation of phase equilibria by linear programming: tool for geodynamic modelling and its application to subduction zone decarbonation. *Earth Planet Sci Lett* 236:524–541
- Connolly JAD (2009) The geodynamic equation of state: what and how. *Geochem Geophys Geosyst* 10:Q10014. <https://doi.org/10.1029/2009GC002540>
- de Wet AP, Miller JA, Bickle MJ, Chapman HJ (1989) Geology and geochronology of the Arnea, Sithonia and Ouranopolis intrusions, Chalkidiki Peninsula, northern Greece. *Tectonophysics* 161(1–2):65–79
- Dimitriadis S, Godelitsas A (1991) Evidence of high-pressure metamorphism in the Vertiskos group of the Serbomacedonian Massif. The eclogite of Nea Roda Chalkidiki. *Bull Geol Soc Greece* XXV(2):67–80
- Dinter D (1998) Late Cenozoic extension of the Alpine collisional orogen, northeastern Greece: origin of the north Aegean basin. *Geol Soc Am Bull* 110:1208–1230

- Dixon JE, Dimitriadis S (1984) Metamorphosed ophiolitic rocks from the SerboMacedonian Massif, near Lake Volvi, North-east Greece. *Geol Soc Lond Spec Publ* 17:603–618
- Dixon JE, Dimitriadis S (1987) The metamorphic evolution of Serbo-macedonian Massif in Greece. *Terra Cognita* 7(2/3):106
- Froitzheim N, Jahn-Awe S, Frei D, Wainwright AN, Maas D, Georgiev N, Nagel TJ, Pleuger J (2014) Age and composition of meta-ophiolite from the Rhodope Middle Allochthon (Satovcha, Bulgaria): a test for the maximum-allochthony hypothesis of the Hellenides. *Tectonics* 33:1477–1500
- Gallhofer D, von Quadt A, Stefan M, Schmid S, Guillong M, Irena Peytcheva I, Seghedi I (2017) Magmatic and tectonic history of Jurassic ophiolites and associated granitoids from the South Apuseni Mountains (Romania). *Swiss J Geosci* 110:699–719. <https://doi.org/10.1007/s00015-016-0231-6>
- Gautier P, Bosse V, Cherneva Z, Didier A, Gerdjikov I, Tiepolo M (2017) Polycyclic alpine orogeny in the Rhodope metamorphic complex: the record in migmatites from the Nestos shear zone (N. Greece). *Bull Soc Géol Fr* 188:36
- Georgiev N, Froitzheim N, Cherneva Z, Frei D, Grozdev V, Silke Jahn-Awe S, Nagel T (2016) Structure and U–Pb zircon geochronology of an Alpine nappe stack telescoped by extensional detachment faulting (Kulidzhik area, Eastern Rhodopes, Bulgaria). *Int J Earth Sci (geol Rundsch)* 105:1985–2012
- Georgieva M, Bosse V, Cherneva Z, Gautier P, Gerdjikov I, Tiepolo M (2010) Late-Jurassic granulite facies metamorphism of garnet-bearing metabasic rocks from the Chepelare area, Central Rhodope. In: *Proceedings of National Conference “Geosciences 2010”*, pp 31–32
- Himmerkus F, Reischmann T, Kostopoulos D (2009a) Serbo-Macedonian revisited: a Silurian basement terrane from northern Gondwana in the internal Hellenides, Greece. *Tectonophysics* 473:20–35. <https://doi.org/10.1016/j.tecto.2008.10.016>
- Himmerkus F, Reischmann T, Kostopoulos D (2009b) Triassic rift-related metagranites in the internal Hellenides. *Greece Geol Mag* 146:252–265
- Himmerkus F, Zachariadis P, Reischmann T, Kostopoulos D (2012) The basement of the Mount Athos peninsula, northern Greece: insights from geochemistry and zircon ages. *Int J Earth Sci* 101:1467–1485
- Ivanova D, Bonev N, Chatalov A (2015) Biostratigraphy and tectonic significance of lowermost Cretaceous carbonate rocks of the Circum–Rhodope Belt (Chalkidiki Peninsula and Thrace region, NE Greece). *Cretac Res* 52:25–63
- Jahn-Awe S, Pleuger J, Frei D, Georgiev N, Froitzheim N, Nagel TJ (2012) Time constraints for low-angle shear zones in the Central Rhodopes (Bulgaria) and their significance for the exhumation of high-pressure rocks. *Int J Earth Sci* 101:1971–2004
- Jahn-Awe S, Froitzheim N, Nagel TJ, Frei D, Georgiev N, Pleuger J (2010) Structural and geochronological evidence for Paleogene thrusting in the Western Rhodopes (SW Bulgaria): elements for a new tectonic model of the Rhodope Metamorphic Province. *Tectonics* 29:TC3008
- Janák M, Froitzheim N, Georgiev N, Nagel TJ, Sarov S (2011) P–T evolution of kyanite eclogite from the Pirin Mountains (SW Bulgaria): implications for the Rhodope UHP metamorphic complex. *J Metamorph Geol* 29:317–332
- Kilias A, Frisch W, Avgerinas A, Dunkl I, Falalakis G, Gawlick HJ (2010) Alpine architecture and kinematics of deformation of the northern Pelagonian nappe pile in the Hellenides. *Austr J Earth Sci* 103(1):4–28
- Kirchenbauer M, Munker C, Schuth S, Garbe-Schönberg D, Marchev P (2012) Tectonomagmatic constraints on the sources of eastern Mediterranean K-rich lavas. *J Petrol* 53:27–65
- Kockel F, Mollat H (1977) Geological map of the Chalkidiki peninsula and adjacent areas (Greece), Scale 1:100000. Bundesanstalt für Geowissenschaften und Rohstoffe, Hannover
- Kockel F, Mollat H, Walther H (1977) Erleuterungen zur Geologischen Karte der Chalkidiki und angrenzender Gebiete. Hannover, Bundesanstalt für Geowissenschaften und Rohstoffe, p 119
- Kockel F, Mollat H, Antoniadis P (1978a) Geological map of Greece, 1:50000 sheet Arnaea, IGMR, 1978
- Kockel F, Mollat H, Antoniadis P (1978b) Geological map of Greece, 1:50000 sheet Ierissos, IGMR, 1978
- Kockel F, Mollat H, Walther H, (1978c) Geological map of Greece, 1:50000 sheet Stavros, IGMR, 1978
- Krenn K, Bauer C, Proyer A, Klötzli U, Hoinkes G (2010) Tectonometamorphic evolution of the Rhodope orogen. *Tectonics* 29:TC4001
- Krohe A, Mposkos E (2002) Multiple generations of extensional detachments in the Rhodope Mountains (N. Greece): evidence of episodic exhumation of high-P rocks. In: Blundell DJ, Neubauer G, Von Quant A (eds) *The timing and location of major ore deposits in an evolving orogen*, vol 204. Geological Society of London Special Publication, pp 151–178
- Kydonakis K, Gallagher K, Brun J-P, Jolivet M, Gueydan F, Kostopoulos D (2014) Upper Cretaceous exhumation of the western Rhodope Metamorphic Province (Chalkidiki Peninsula, northern Greece). *Tectonics* 33:1113–1132
- Kydonakis K, Moulas E, Chatzitheodoridis E, Brun J-P, Kostopoulos D (2015) First report on Mesozoic eclogite-facies metamorphism preceding Barrovian overprint from the western Rhodope (Chalkidiki, northern Greece). *Lithos* 220–223:147–163
- Kydonakis K, Brun J-P, Poujol M, Monié P, Chatzitheodoridis E (2016) Inferences on the Mesozoic evolution of the North Aegean from the isotopic record of the Chalkidiki block. *Tectonophysics* 682:65–84. <https://doi.org/10.1016/j.tecto.2016.06.006>
- Leake B (1997) Nomenclature of amphiboles: report of the subcommittee on amphiboles of the international mineralogical association, commission on new minerals and mineral names. *Can Miner* 35:219–246
- Liati A, Gebauer D, Wysoczanski R (2002) U–Pb SHRIMP-dating of zircon domains from UHP garnet-rich mafic rocks and late pegmatoids in the Rhodope zone (N Greece); evidence for Early Cretaceous crystallization and Late Cretaceous metamorphism. *Chem Geol* 184:281–299
- Liati A, Theye T, Fanning CM, Gebauer D, Rayner N (2016) Multiple subduction cycles in the Alpine orogeny, as recorded in single zircon crystals (Rhodope zone, Greece). *Gondwana Res* 29:199–207
- Liati A, Gebauer D, Fanning M (2011) Geochronology of the Alpine UHP Rhodope zone: a review of isotopic ages and constraints on the geodynamic evolution. In: Dobrzhinetskaya et al. (ed), *Ultrahigh-Pressure Metamorphism. 25 years after the discovery of coesite and diamond*, Elsevier, pp 295–324
- Massonne H-J, Schreyer W (1987) Phengite geobarometry based on the limited assemblage with K-feldspar, phlogopite and quartz. *Contrib Mineral Petrol* 96:212–224
- Meinhold G, Kostopoulos D (2013) The Circum–Rhodope belt, northern Greece: age, provenance, and tectonic setting. *Tectonophysics* 595–596:55–68
- Meinhold G, Kostopoulos D, Reischmann T, Frei D, BouDagher-Fadel MK (2009) Geochemistry, provenance and stratigraphic age of metasedimentary rocks from the eastern Vardar suture zone, northern Greece. *Palaeogeogr Palaeoclimatol Palaeoecol* 277(3–4):199–225
- Mercier J (1968) Etude géologique des zones Internes des Hellenides en Macedoine centrale Contribution a l’ etude du Metamorphisme et de l’ evolution magmatique des Zones Internes des Hellenides. *Ann Geol Pays Hellenic* 20:1–739

- Mercier J, Vergely P (1994) Is the Paikon Massif a tectonic window in the Axios-Vardar zone? (Internal Hellenides, Macedonia Greece). *Bull Geol Soc Greece* XXX(1):115–120
- Michard A, Goffé B, Liati A, Mountrakis D (1994) Blueschist-facies assemblages in the peri-Rhodopian zone, and hints for an Eohellenic HP-LT belt in northern Greece. *Bull Geol Soc Greece* XXX:185–192
- Miladinova I, Froitzheim N, Nagel T, Janak M, Georgiev N, Fonseca R, Sandmann SN, Mönker C (2018) Late Cretaceous eclogite in the Eastern Rhodopes (Bulgaria): evidence for subduction under the Sredna Gora magmatic arc. *Int J Earth Sci* 107:2083–2099. <https://doi.org/10.1007/s00531-018-1589-7>
- Mposkos E, Krohe A (2006) Pressure-temperature-deformation paths of closely associated ultra-high pressure (diamond-bearing) crustal and mantle rocks of the Kimi complex: implications for the tectonic history of the Rhodope Mountains, northern Greece. *Can J Earth Sci* 43:1755–1776
- Mposkos E, Wawrzenitz N (1995) Metapegmatites and Pegmatites bracketing the time of HP-metamorphism in polymetamorphic rocks of the E-Rhodope, N-Greece. *Geol Soc Greece Spec Publ* 4(2):602–608
- Mposkos E, Kostopoulos D, Krohe A (2001) Low-P/high-P pre-Alpine metamorphism and Medium-P Alpine overprint of the Pelagonian zone documented in high-alumina metapelites from the Vernon Massif, western Macedonia northern Greece. *Bull Geol Soc Greece* XXXIV:949–958
- Mposkos E, Baziotis I, Proyer A (2012) Pressure-temperature evolution of eclogites from the Kechros complex in the Eastern Rhodope (NE Greece). *Int J Earth Sci* 101:973–996
- Mposkos E, Krohe A (2000) Petrological and structural evolution of continental high pressure (HP) metamorphic rocks in the Alpine Rhodope Domain (N.Greece). In: Panayides I, Xenophontos C, Malpas J (ed.), Proceedings of the 3rd International Conference on the Geology of the Eastern Mediterranean, Nicosia, Cyprus, 1999. Geological Survey, Nicosia, Cyprus, pp 221–232
- Mposkos E, Krohe A (2004) New evidences of the low-P/high-T pre-Alpine metamorphism and medium-P Alpine overprint of the pelagonian zone documented in metapelites and orthogneisses from the Vores Massif, Macedonia, northern Greece. In: Bulletin of the Geological Society of Greece vol. XXXVI, 2004 Proceedings of the 10th International Congress, Thessaloniki, April 2004
- Mposkos E, Krohe A, Baziotis I (2021) Deep tectonics in the eastern hellenides uncovered: the record of Variscan continental amalgamation, Permo-Triassic rifting, and early Alpine Collision in pre-Variscan continental crust in the W-Rhodope (Vertiscos-Ograzden Complex, N-Greece). *Tectonics* 40(2):e2019TC005557
- Mussallam K, Jung D (1986) Petrology and geotectonic significance of salic rocks preceding ophiolites in the Eastern Vardar Zone, Greece. *TMPM Tschermaks Min P Etr Mitt* 35:217–242
- Nagel TJ, Schmidt S, Janák M, Froitzheim N, Jahn-Awe S, Georgiev N (2011) The exposed base of a collapsing wedge—The Nestos Shear Zone (Rhodope Metamorphic Province, Greece). *Tectonics* 30:TC4009. <https://doi.org/10.1029/2010TC002815>
- Nitra G, Moratti G, Piccardi L, Montanari D, Carras N, Catanzariti R, Chiari M, Marcucci M (2018) From obduction to continental collision: new data from Central Greece. *Geol Mag* 155:377–421. <https://doi.org/10.1017/S0016756817000942>
- Oh CW, Liou JG (1998) A petrogenetic grid for eclogite and related facies under high-pressure metamorphism. *The Island Arc* 7:36–51
- Petrík I, Janák M, Froitzheim N, Georgiev N, Yoshida K, Sasinková V, Konečný P, Milovská S (2016) Triassic to early Jurassic (c. 200 Ma) UHP metamorphism in the Central Rhodopes: evidence from U–Pb–Th dating of monazite in diamond-bearing gneiss from Chepelare (Bulgaria). *J Metamorph Geol* 34:265–291
- Peytcheva I, Macheva L, von Quadt A, Zidarov N (2015) Gondwana-derived units in Ograzhden and Belasitsa Mountains, Serbo-Macedonian Massif (SW Bulgaria): combined geochemical, petrological and U–Pb zircon-xenotime age constraints. *Geologica Balcanica* 44:51–84
- Pleuger J, Cherneva Z, Klug L, Hoffmann E, Schmidtke M, Froitzheim N, Georgiev N, Naydenov K, Stegmann K, Pohl A, Germer M, Borchert A, Menneken M (2020) The Neotethys suture in the eastern Bulgarian Rhodopes.
- Ricou LE, Burg JP, Godfriaux I, Ivanov Z (1998) Rhodope and Vardar: the metamorphic and olistostromic paired belts related to Cretaceous subduction under Europe. *Geodyn Acta* 11:285–309
- Sakellariou D, Dürr S (1993) Geological structure of the Serbo-Macedonian massif in NE Chalkidiki peninsula. *Bull Geol Soc Greece* XXVIII(1):179–193
- Schenker FL (2013) Thermo-mechanical evolution of the Pelagonian Gneiss Dome (Greece): Insights from numerical modeling and new geological and geochronological data. In: Ph.D. ETH Zurich NO. 21010, p 448
- Schmid SM, Fügenschuh B, Kunov A, Mačenco L, Nievergelt P, Oberhänsli R, Pleuger J, Schefer S, Schuster R, Tomljenović B, Ustaszewski K, van Hinsbergen D (2020) Tectonic units of the Alpine collision zone between Eastern Alps and western Turkey. *Gondwana Res* 78:308–374
- Sharp IR, Robertson AHF (2006) Tectonic-sedimentary evolution of the western margin of the Mesozoic Vardar Ocean: evidence from the Pelagonian and Almopias zones, northern Greece. *Geol Soc Lond Spec Publ* 260:373–412. <https://doi.org/10.1144/GSL.SP.2006.260.01.16>
- Sunal G, Sarir M, Natalin BA, Topuz G, Vonderschmidt O (2011) Metamorphism and diachronous cooling in a contractional orogen: the Strandja Massif, NW Turkey. *Geol Mag* 148:580–596
- Tranos M, Kilias A, Mountrakis D (1999) Geometry and kinematics of the tertiary postmetamorphic Circun Rhodope belt thrust system (CRTBS), Northern Greece. *Bull Geol Soc Gr* 33:5–16
- Trapp S, Janák M, Fassmer K, Froitzheim N, Münker C, Georgiev N (2020) Variscan ultra-high-pressure eclogite in the Upper Allochthon of the Rhodope Metamorphic Complex (Bulgaria). *Terra Nova* 33(2):174–183
- Turpaud P, Reischmann T (2010) Characterisation of igneous terranes by zircon dating: Implication for UHP occurrences and suture identification in the central Rhodope, northern Greece. *Int J Earth Sci* 99:567–591
- von Quadt A, Sarov S, Peytcheva I, Voinova E (2009) Jurassic meta-granitoids south of the West-Rhodope batholith-conventional and in situ U–Pb zircon analyses, Sr–Nd–Hf isotope tracing and geodynamic constraints. *Geosciences* 2009:11–12
- Wawrzenitz N, Krohe A, Baziotis I, Mposkos E, Kylander-Clark A, Romer RL (2015) LASS U–Th–Pb monazite and rutile geochronology of felsic high-pressure granulites (Rhodope, N Greece): the role of fluids, deformation and metamorphic. *Lithos* 232:266–285
- Whitney D, Evans B (2010) Abbreviations for names of rock-forming minerals. *Am Miner* 95:185–187
- Wuthrich E (2009) Low temperature thermochronology of the North Aegean Rhodope Massif. In: PhD thesis, Swiss Federal Institute of Technology, Zurich
- Zachariadis P (2007) Ophiolites of the Eastern Vardar Zone, N. Greece. In: Universität Mainz, Germany (Ph.D. thesis)
- Zachariadou S, Dimitriadis S (1994) Crustal extension and partial melting possibly related to the opening of a marginal basin. The polytictic migmatites of Piyi and Karathodoro Macedonia Greece. *Bull Geol Soc Greece* 1(1):271–284